Chapter 3
Electrodeposition of Copper Powders and Their Properties

Nebojša D. Nikolić and Konstantin I. Popov

3.1 Introduction

A powder is a finely divided solid, smaller than 1,000 μm in its maximum dimension. A particle is defined as the smallest unit of a powder. The particles of a powder may assume various forms and sizes, whereas powders, an association of such particles, exhibit, more or less, the same characteristics as if they were formed under identical conditions and if the manipulation of the deposits after removal from the electrode was the same [1, 2]. The size of particles of many metal powders can vary in a quite wide range from a few nanometers to several hundreds of micrometers. The most important properties of a metal powder are the specific surface, the apparent

N.D. Nikolić (✉)
ICTM-Institute of Electrochemistry, University of Belgrade, Njegoševa 12, P.O.B. 473,11001 Belgrade, Serbia
e-mail: nnikolic@tmf.bg.ac.rs

K.I. Popov
ICTM-Institute of Electrochemistry, University of Belgrade, Njegoševa 12, P.O.B. 473,11001 Belgrade, Serbia

Faculty of Technology and Metallurgy, University of Belgrade, Karnegijeva 4, P.O.B. 3503,11001 Belgrade, Serbia
e-mail: kosta@tmf.bg.ac.rs

density, the flowability, and the particle grain size and distribution. These properties, called decisive properties, characterize the behavior of a metal powder.

Different methods for the production of metal powders including mechanical commuting, chemical reaction, electrolysis, and liquid metal atomization are used in practice [1]. Powders of about 60 metals can successfully be produced by electrolysis. The majority of metallic powders are obtained by molten-salts electrolysis. However, due to technological advantages and various industrial applications most of the practically useful powders, e.g., copper, iron, and nickel, are produced from aqueous solutions [3].

Electrodeposited metallic powders are mainly produced in a dendritic form. The dendrites can spontaneously fall off or can be removed from the electrode by tapping or other similar techniques. Also, the powders are obtained as flakes or needles, fibrous or spongy forms, etc., depending on the conditions of electrodeposition and on the nature of the metal.

The formation of powders by electrolysis is an economical processing method with a low capital investment and operational cost. The main advantages of this method in relation to other methods of metal powder production are high purity of the produced powder, which can be easily pressed and sintered, and low oxygen content [1, 2]. It is environmentally a friendly way of powder production which enables working in a closed circuit [4]. Metal powders can be formed by both potentiostatic and galvanostatic regimes of electrolysis [2, 5, 6]. In addition, metal powders can be produced under periodically changing regimes of electrolysis, such as pulsating overpotential (PO), pulsating current (PC), and reversing current (RC) [5, 6].

3.1.1 Formation of Metal Powders by Electrolysis: Comparison of Potentiostatic and Galvanostatic Regimes

All metals which can be electrodeposited exhibit a tendency to appear in the form of powders at current densities larger than a certain critical value, j_{cr}. This value is equal to the limiting diffusion

current density in galvanostatic deposition, as shown by Hirakoso [7, 8] and Ibl [9, 10]. At the same time Kudra et al. [11, 12] observed that the product of the current density used and the square root of the time of powder formation t_i is a constant quantity. The time for powder formation at current densities equal to j_{cr} and larger can be observed visually as the electrode is seen to turn suddenly from a lustrous to a black appearance. During this induction period a compact deposit is formed. Ibl and Schadegg [13] showed that at sufficiently high deposition times, powdered deposits can be obtained at all overpotentials which correspond to the limiting diffusion current plateau. It is known that the limiting diffusion current plateau covers a wide range of overpotentials, because of a large change of overpotential for extremely small changes of current density. Therefore, as pointed out by Calusaru [3], the formation of electrolytic powder cannot be localized at a certain point on the current density versus polarization curve by using only current density measurements. Calusaru et al. [3, 14, 15] showed that there are three ranges of overpotential which can be determined from studies of deposit structure. Similar facts were reported by Russev [16] and Theis et al. [17]. According to Calusaru [3], there are regions of overpotential in which compact, rough, and really powdered deposits are obtained. Popov et al. [18] showed that in potentiostatic deposition two critical values of overpotential can be determined: the critical overpotential for dendrite growth initiation, η_i, and the critical overpotential for powder formation, η_c. Simultaneously, it was shown that dendritic deposits are obtained at all overpotentials between η_i and η_c after a sufficiently long induction period, which is in agreement with the findings of Ibl and Schadegg [13]. Also, it was shown [3] that during potentiostatic deposition with sufficiently long deposition times, dendritic and powdered deposits can be obtained at current densities lower than the limiting diffusion value. This is not possible in the case of galvanostatic deposition.

According to Popov et al. [18], the minimum overpotential at which dendritic growth, η_i, is possible at a macroelectrode is given by

$$\eta_i = \frac{b_c}{2.3} \ln \frac{4j_L}{j_0} + \Delta \eta \qquad (3.1)$$

and the minimum overpotential at which instantaneous dendritic growth, η_c, is possible is given by

$$\eta_c = \frac{b_c}{2.3} \ln \frac{j_L \delta}{j_0 h_0} + \Delta \eta, \tag{3.2}$$

where b_c is the cathodic Tafel slope, j_L is the limiting diffusion current density, j_0 is the exchange current density, δ is the diffusion layer thickness, and h_0 is the initial protrusion height.

$\Delta \eta$ in Eqs. (3.1) and (3.2) represents the difference in the reversible potential of the tip of the dendrite and a planar surface [19], and it is presented by Eq. (3.3):

$$\Delta \eta = \frac{2\sigma V}{nFR}, \tag{3.3}$$

where nF is the number of Faradays per mole of consumed ions, R is the molar gas constant, V is the molar volume of deposited metal, and σ is the interfacial energy between metal and solution. $\Delta \eta$ is the order of a few millivolts and it can be neglected in the consideration of both η_i and η_c overpotentials. Also, the following forms of Eqs. (3.1) and (3.2) are often found in the literature: [5]

$$\eta_i = \frac{b_c}{2.3} \ln \frac{j_L}{j_0} \tag{3.4}$$

and

$$\eta_c = \frac{b_c}{2.3} \ln \frac{j_L \delta}{j_0 h_0}. \tag{3.5}$$

The relationship between overpotential and current density in mixed controlled metal electrodeposition is given by

$$\eta = \frac{b_c}{2.3} \ln \frac{j}{j_0} \frac{1}{(1 - j/j_L)}, \tag{3.6}$$

where j is the current density of electrodeposition.

Current densities j_i and j_{cr} which correspond to η_i and η_c can be obtained by eliminating η from (3.1), (3.2), and (3.6) as[1]

$$j_i = 0.8 j_L \tag{3.7}$$

and

$$j_{cr} = \frac{j_L(\delta/h_0)}{1 + (\ \delta/h_0)} \tag{3.8}$$

or

$$j_i = j_L \tag{3.9}$$

for $\delta/h_0 \gg 1$. Hence, it can be concluded that dendritic growth is not possible at [19]

$$j < j_i \tag{3.10}$$

but growth is possible after an induction time at

$$j_i \leq j < j_L \tag{3.11}$$

and instantaneous growth is possible at

$$j \geq j_L \tag{3.12}$$

in potentiostatic electrodeposition. The fact that dendritic growth in potentiostatic deposition is possible at $\eta < \eta_c$, and hence $j < j_L$, (regardless $j \sim j_L$), was explained by the effect of nondendritic surface roughness amplification during the induction time of dendritic growth [18].

This effect in galvanostatic electrodeposition will be in the opposite direction. It was shown by Maksimović et al. [20, 21] that the

---

[1] The elimination η from Eqs. (3.4) to (3.6), $j_i = 0.5\ j_L$, and this dependence can also be found in the literature.
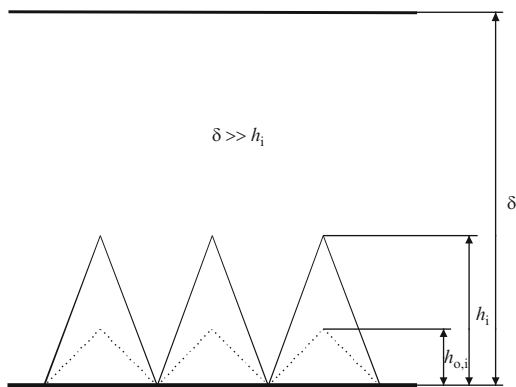
Fig. 3.1 Schematic representation of a rough electrode surface area

surface roughness amplification of a protrusion with an initial height, h_0, in galvanostatic deposition (for $t \ll \tau$) obeys the same relation as in the case of potentiostatic electrodeposition [22–27], i.e.,

$$h = h_0 \exp(t/\tau), \tag{3.13}$$

where $\tau = (\delta^2/V_m D C_0)$, if the condition $\delta \gg h$ is satisfied. In Eq. (3.13), D is diffusion coefficient and C_o is the bulk concentration. It is easy to show that for the electrode surface presented in Fig. 3.1, the real electrode surface area will increase with time according to

$$S = S_0 \exp(t/\tau) \tag{3.14a}$$

since

$$S = k \sum_{i=1}^{N} h_i \tag{3.14b}$$

and

$$S_0 = k \sum_{i=1}^{N} h_{0,i}. \tag{3.14c}$$

Obviously, the real current density will decrease according to

$$j = j^0 \exp(-t/\tau), \qquad (3.15)$$

where j^0 is initial current density, while the overpotential will decrease according to

$$\eta = \frac{b_c}{2.3} \ln \frac{j^0 \exp(-t/\tau)j_L}{j_0[j_L - j^0 \exp(-t/\tau)]}, \qquad (3.16)$$

where Eq. (3.16) is obtained by substitution of j from Eq. (3.15) into Eq. (3.6).

The critical overpotential for instantaneous dendritic growth is given by Eq. (3.5) for protrusions with an initial height h_0. In potentiostatic deposition, an overpotential lower than η_c can belong to the limiting diffusion range. Nondendritic surface roughness amplification in the limiting diffusion current density range does not depend on overpotential, leading to an increase of height of the protrusion. Substitution of h from Eq. (3.13) in Eq. (3.5) shows the change of critical overpotential of instantaneous dendritic growth with time caused by nondendritic surface roughness amplification as

$$\eta_{c,t} = \frac{b_c}{2.3} \ln \frac{j_L \delta}{j_0 h} = \eta_c - \frac{b_c}{2.3} \frac{t}{\tau}. \qquad (3.17)$$

Hence, the overpotential of deposition remains constant and the critical overpotential of instantaneous dendritic growth decreases, and at $t = t_i$ these values become equal and dendritic growth starts. In galvanostatic conditions, nondendritic amplification causes a decrease in the critical overpotential for dendritic growth according to Eq. (3.17), but at the same time the overpotential of deposition decreases according to Eq. (3.16). The time t_i in which these two overpotentials become equal can be obtained by the elimination of η from Eqs. (3.16) and (3.17) as

$$t_i = -2.3\tau \log \frac{j_L}{j^0} \qquad (3.18)$$

if $\delta \gg h_0$. Hence, $t_i = 0$ for $j^0 = j_L$ and instantaneous dendritic growth is possible; at $j^0 < j_L$, for $t_i < 0$ dendritic growth is not possible. In this way, the induction period for the dendritic growth becomes equal to the transition time.

The above discussion is valid for galvanostatic powder electrode-position. Due to the increase in real surface area of the electrode, the working current density should be many times larger than limiting diffusion one [28]. In this way, the decrease in the current density below the limiting diffusion one can be avoided. Hence, hydrogen codeposition in galvanostatic powder electrodeposition is inevitable. The situation is somewhat different under the potentiostatic conditions. In this regime, dendrites of deposited metal also appear in the limiting diffusion current density range. For some metals, however, hydrogen codeposition is not a necessary factor influencing the powder formation [5, 29]. In the absence of vigorous hydrogen evolution, powder particles are well-developed dendrites or parts of them. At overpotentials larger than that of vigorous hydrogen evolution, the conditions of the powder formation become similar to those in galvanostatic deposition.

There are at least two basic consequences of the vigorous hydrogen evolution during the metal powder particle formation. First, the hydro-dynamic regime in the vicinity of the electrode can be changed due to stirring of the solution by evolved hydrogen, thus resulting in the increase of the limiting diffusion current density [30]. This causes the formation of morphological forms appearing before dendrite growth initiation at specified overpotential. Second, the formation of hydrogen bubbles strongly influences the current density distribution over electrode surface and hence the powder particle formation [31, 32].

3.2 Copper Powdered Deposits

3.2.1 Basic Facts

The most often employed electrolytes for the electrodeposition of copper are those based on aqueous solutions of cupric sulfate ($CuSO_4$) and sulfuric acid (H_2SO_4) [33]. There is an ionic equilibrium of a
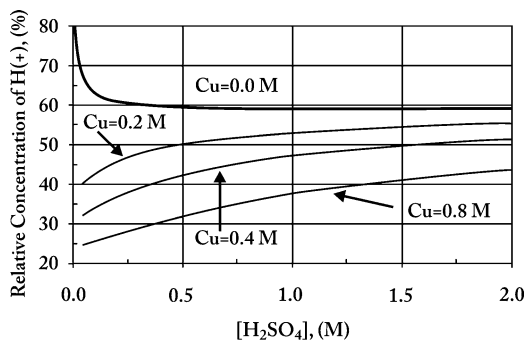
Fig. 3.2 Relative concentration of hydrogen ions as a function of sulfuric acid and total copper concentrations, at 25°C ($C_{RH+} = [H^+]/[H_T]$) (Reprinted from [36] with permission from Elsevier and [38] with permission from Springer.)

lot of species, such as bisulfate ions (HSO_4^-), cupric ions (Cu^{2+}), aqueous cupric sulfate ($CuSO_{4(aq)}$), hydrogen ions (H^+), and sulfate ions (SO_4^{2-}), in the $CuSO_4$–H_2SO_4–H_2O system [34–36]. Using Pitzer's model [37], the ionic equilibrium of these species over a wide range of concentrations and temperatures was calculated [36], and the dependence of the relative concentration of hydrogen ions (H^+) on H_2SO_4 concentration for different copper concentration is shown in Fig. 3.2. From Fig. 3.2, it can be seen that increasing the copper concentration produces a sharp decrease in the hydrogen ion concentration, while increasing the concentration of sulfuric acid produces an increase in the hydrogen ion concentration [36].

Irregular or powdered copper deposits are formed by electrodeposition from acid sulfate solutions at current densities and overpotentials corresponding to the plateau of the limiting diffusion current density and at higher ones. At these overpotentials and current densities, parallel to copper electrodeposition processes, hydrogen evolution reaction occurs [30]. Hence, it is very clear that the formation of powdered copper deposits is closely related with hydrogen evolution reaction as the second reaction in copper electrochemical deposition processes at high overpotentials and current densities [38].

Due to the ionic equilibrium of the species in the $CuSO_4$–H_2SO_4–H_2O system (Fig. 3.2), the quantities of evolved hydrogen and hence morphologies of powdered copper deposits depend strongly on the
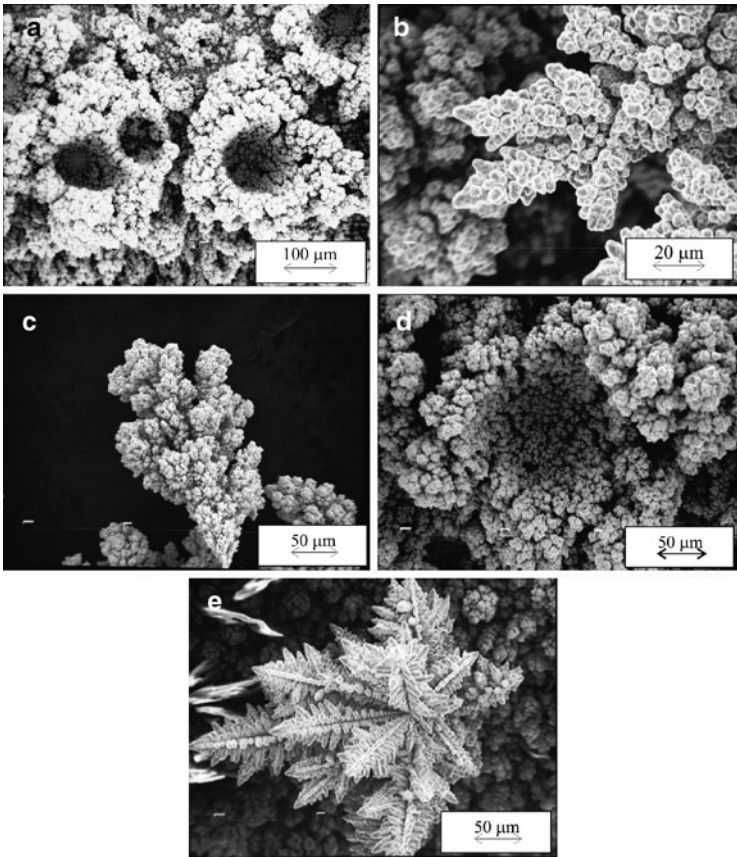
Fig. 3.3 Copper deposits obtained at an overpotential of 800 mV from (**a**) 0.075 M CuSO$_4$ in 0.50 M H$_2$SO$_4$; (**b**)–(**d**) 0.30 M CuSO$_4$ in 0.50 M H$_2$SO$_4$; and (**e**) 0.60 M CuSO$_4$ in 0.50 M H$_2$SO$_4$ (Reprinted from [39] with permission from Elsevier and [38] with permission from Springer.)

used concentrations of CuSO$_4$ and H$_2$SO$_4$ [39, 40]. Figure 3.3 shows copper deposits obtained by potentiostatic electrodepositions at an overpotential of 800 mV from copper solutions containing 0.075, 0.30, and 0.60 M CuSO$_4$ in 0.50 M H$_2$SO$_4$. For all these solutions, an overpotential of 800 mV was about 50 mV outside the plateau of the limiting diffusion current density [31, 39]. The quantities of

hydrogen generated during electrodeposition processes at 800 mV from these solutions corresponded to the average current efficiencies of hydrogen evolution, $\eta_{I,av}(H_2)$, of 42.2% for 0.075 M $CuSO_4$ in 0.50 M H_2SO_4 (the ratio of $CuSO_4/H_2SO_4 = 0.15$), 3.5% for 0.30 M $CuSO_4$ in 0.50 M H_2SO_4 (the ratio of $CuSO_4/H_2SO_4 = 0.60$), and 0.66% for 0.60 M $CuSO_4$ in 0.50 M H_2SO_4 (the ratio of $CuSO_4/H_2SO_4 = 1.2$) [39].

The honeycomb-like structure was formed by electrodeposition from 0.075 M $CuSO_4$ in 0.50 M H_2SO_4 (Fig. 3.3a). A mixture of dendritic forms (Fig. 3.3b), degenerate dendrites (Fig. 3.3c), and holes formed due to the attached hydrogen bubbles (Fig. 3.3d) was obtained by electrodeposition from 0.30 M $CuSO_4$ in 0.50 M H_2SO_4. Finally, very branchy dendrites were formed by electrodeposition from 0.60 M $CuSO_4$ in 0.50 M H_2SO_4 (Fig. 3.3e). It is very clear that the change of morphology of electrodeposited copper with the increasing Cu(II) ions concentration is a consequence of the decrease of effectiveness of solution stirring by evolved hydrogen caused by the decrease of the relative concentration of H^+ ions with the increase of Cu concentration (Fig. 3.2). The critical quantity of evolved hydrogen which causes the effective solution stirring and leads to the change of hydrodynamic conditions in the near-electrode layer was estimated to correspond to $\eta_{I,av}(H_2)$ of 10.0% [31]. For the H_2SO_4 concentration of 0.50 M, the maximal concentration of Cu(II) ions enabling the formation of the honeycomb-like structures is estimated to correspond to 0.15 M $CuSO_4$ [31].

This is a vertical analysis of the ionic equilibrium of species in the $CuSO_4$–H_2SO_4–H_2O system. Horizontal analysis of this equilibrium is made keeping the Cu(II) ions constant and varying H_2SO_4 concentrations. Morphologies of electrodeposited copper obtained at an overpotential of 800 mV from 0.15 M $CuSO_4$ in 0.125, 0.25, and 1.0 M H_2SO_4 are shown in Fig. 3.4. For these solutions, an overpotential of 800 mV was about 50 mV outside the plateaus of the limiting diffusion current density [41]. The average current efficiencies of hydrogen evolution, $\eta_{I,av}(H_2)$, were 4.83% (for the copper solution containing 0.15 M $CuSO_4$ in 0.125 M H_2SO_4; the $CuSO_4/H_2SO_4$ ratio = 1.2), 9.05% (for the copper solution containing 0.15 M $CuSO_4$ in 0.25 M H_2SO_4; the $CuSO_4/H_2SO_4$ ratio = 0.60), and 23.3% (for the copper solution containing
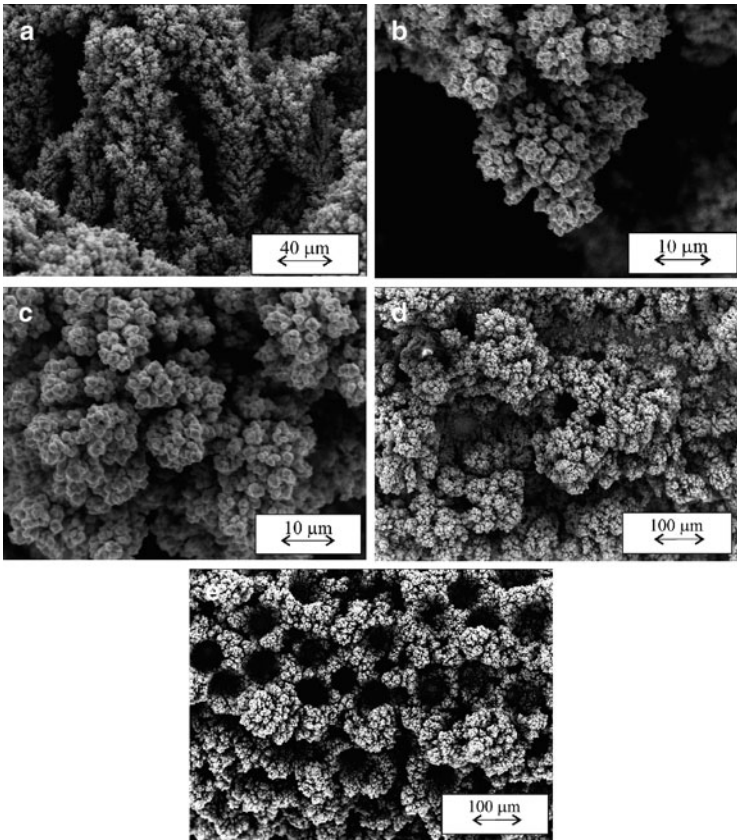
Fig. 3.4 Copper deposits obtained at an overpotential of 800 mV from: (**a**)–(**c**) 0.15 M CuSO$_4$ in 0.125 M H$_2$SO$_4$; (**d**) 0.15 M CuSO$_4$ in 0.25 M H$_2$SO$_4$; and (**e**) 0.15 M CuSO$_4$ in 1.0 M H$_2$SO$_4$ (Reprinted from [39] with permission from Elsevier and [38] with permission from Springer.)

0.15 M CuSO$_4$ in 1.0 M H$_2$SO$_4$; the CuSO$_4$/H$_2$SO$_4$ ratio = 0.15) [39]. Please note that the same CuSO$_4$/H$_2$SO$_4$ ratios were analyzed in both cases.

A channel structure (Fig. 3.4a), degenerate dendrites (Fig. 3.4b), and cauliflower-like forms (Fig. 3.4c) were formed by copper electro-deposition from 0.15 M CuSO$_4$ in 0.125 M H$_2$SO$_4$. Holes originating

from attached hydrogen bubbles were formed by electrodeposition from 0.15 M $CuSO_4$ in 0.25 M H_2SO_4 (Fig. 3.4d). Degenerate dendrites and cauliflower-like forms, similar to those shown in Fig. 3.4b, c, were also formed by electrodeposition from this solution. Finally, the honeycomb-like structure, constructed from holes formed due to attached hydrogen bubbles and cauliflower-like agglomerates of copper grains between them, was formed by the electrodeposition from 0.15 M $CuSO_4$ in 1.0 M H_2SO_4 (Fig. 3.4e).

The observed morphologies of copper deposits were in a good agreement with the prediction of the ionic equilibrium of the species in the $CuSO_4$–H_2SO_4–H_2O system. The addition of excess H_2SO_4 to the electroplating solution increases the H^+ ion concentration, which is confirmed by the higher values of the average current efficiencies of hydrogen evolution from the solutions with higher concentrations of H_2SO_4 and by the change of copper morphology from cauliflower-like forms and degenerate dendrites to the honeycomb-like structure. For a constant H_2SO_4 concentration, the H^+ ion concentration decreases with increasing copper concentration, which is manifested by the smaller quantity of evolved hydrogen from solutions with higher $CuSO_4$ concentrations and by the change of morphology of electro-deposited copper from the honeycomb-like structure to dendrites [39].

The effect of $CuSO_4$ and H_2SO_4 concentrations on both hydrogen evolution rate and morphology of electrodeposited copper was also observed during electrochemical deposition processes at overpotentials of 650 and 1,000 mV [31, 41, 42]. During electrodeposition processes at 650 mV, the branching of dendrites decreased with the increasing $CuSO_4$ concentration [31], while the number of formed dendritic forms as well as their branching increased with the decrease of H_2SO_4 concentration [41]. Although holes originating due to detachment of hydrogen bubbles were obtained by electrodepositions at 1,000 mV from all analyzed solutions, the number, shape, and size of holes strongly depended on the $CuSO_4$ and H_2SO_4 concentrations used [42].

It is necessary to note that effects on morphology of powdered deposits similar to those obtained by the use of more solutions of different $CuSO_4$ and H_2SO_4 concentrations can be attained by the use of the only one solution if electrodeposition processes were performed at a periodically changing rate.

3.2.2 The Application of Periodically Changing Regimes of Electrolysis in the Formation of Powdered Deposits

Electrodeposition at a periodically changing rate is based on the periodic repetition of current or overpotential waves [27, 43]. The application of periodically changing regimes of electrolysis, such as pulsating overpotential (PO), pulsating (PC), and reversing current (RC), in metal electrodeposition processes is of great academic and practical significance [5, 43]. The most important regime from the theoretical point of view is obviously pulsating overpotential. On the other hand, the most important regime from practical point of view is the reversing current.

Deposition at a periodically changing rate offers a number possibilities for changing the deposition conditions at one and the same deposition rate [43]. Deposits with desired composition, structure, porosity, and hydrogen content, the enhanced throwing power especially in the holes, and the reduction of the use of additives are some of advantages of the use of pulse regimes of electrolysis. From the point of view of powder formation, powder particles with different grain size and morphology can be obtained by varying the wave of periodically changing current or overpotential [6].

In the hydrogen codeposition range, the effect of the PO regime on microstructural characteristics of the honeycomb-like structures was similar to those attained by the application of additives in electrodeposition processes [44–46]. Some of conveniences of the application of these regimes of electrolysis on the formation of various disperse morphological forms of copper can be presented as follows: in this section, the presented copper morphologies were obtained by electrodepositions from 0.15 M $CuSO_4$ in 0.50 M H_2SO_4 by the regime of pulsating current (PC). Electrodepositions were performed at the room temperature using cylindrical copper wires as working electrodes. The current density amplitude of 0.20 A cm^{-2} was used [47].

The first set of experiments was done applying square-waves PC with a constant pause duration, t_p, of 10 ms, and deposition pulses, t_c, of 1, 2, and 50 ms (pause to pulse ratios, p, where $p = t_p/t_c$ were 10, 5, and 0.2, respectively). The average current efficiencies for hydrogen

evolution reaction, $\eta_{I,av}(H_2)$, determined using the experimental procedure adapted to the PC regime were 5.5, 10.3, and 27.2% for pause to pulse ratios of 10, 5, and 0.2, respectively [47].

Morphologies of copper deposits obtained with deposition pulses of 1, 2, and 50 ms and a pause duration of 10 ms are shown in Fig. 3.5. Holes formed by attached hydrogen bubbles, very branchy dendrites, and small agglomerates of copper grains are formed when the applied deposition pulse was 1 ms (Fig. 3.5a, b). The mixture of holes and degenerate dendrites was formed with a deposition pulse of 2 ms (Fig. 3.5c, d). Honeycomb-like copper structure constructed of holes and cauliflower-like agglomerates of copper grains formed around them was obtained with a deposition pulse of 50 ms (Fig. 3.5e, f).

In the second set of experiments, the constant deposition pulse of 10 ms and pause durations of 100, 50, and 2 ms were analyzed (pause to pulse ratios: 10, 5, and 0.2, respectively). In this case, the average current efficiencies for hydrogen evolution reaction, $\eta_{I,av}(H_2)$, were 5.6, 12.4, and 26.8% for duration of pause of 100, 50, and 2 ms, respectively [47]. Morphologies of copper deposits obtained with a deposition pulse of 10 ms and pause durations of 100, 50, and 2 ms are shown in Fig. 3.6. Holes which the walls were constructed of dendrites and dendritic particles formed between holes were primarily formed by square-wave PC with a pause of 100 ms (Fig. 3.6a, b). These copper dendrites were considerably smaller and formed over the whole electrode surface in relation to those formed by the PC regime of the same pause to pulse ratio ($p = 10$) but with a deposition pulse of 1 ms and a pause of 10 ms (Fig. 3.5b). The shortening of pause duration from 100 to 50 ms led to the increase of number of holes formed by attached hydrogen bubbles (Fig. 3.6c), and the change of morphology of electrodeposited copper from dendritic particles to agglomerates consisted of copper grains and rare small dendrites on them (Fig. 3.6d). Finally, the typical honeycomb-like structure is formed with a pause of 2 ms (Fig. 3.6e, f). The increase of the number of holes, as well as the change of morphology of electrodeposited copper from dendrites to agglomerates of copper grains, is a result of the increasing quantity of evolved hydrogen and the increased effectiveness of solution stirring by evolved hydrogen with the shortening of pause duration.
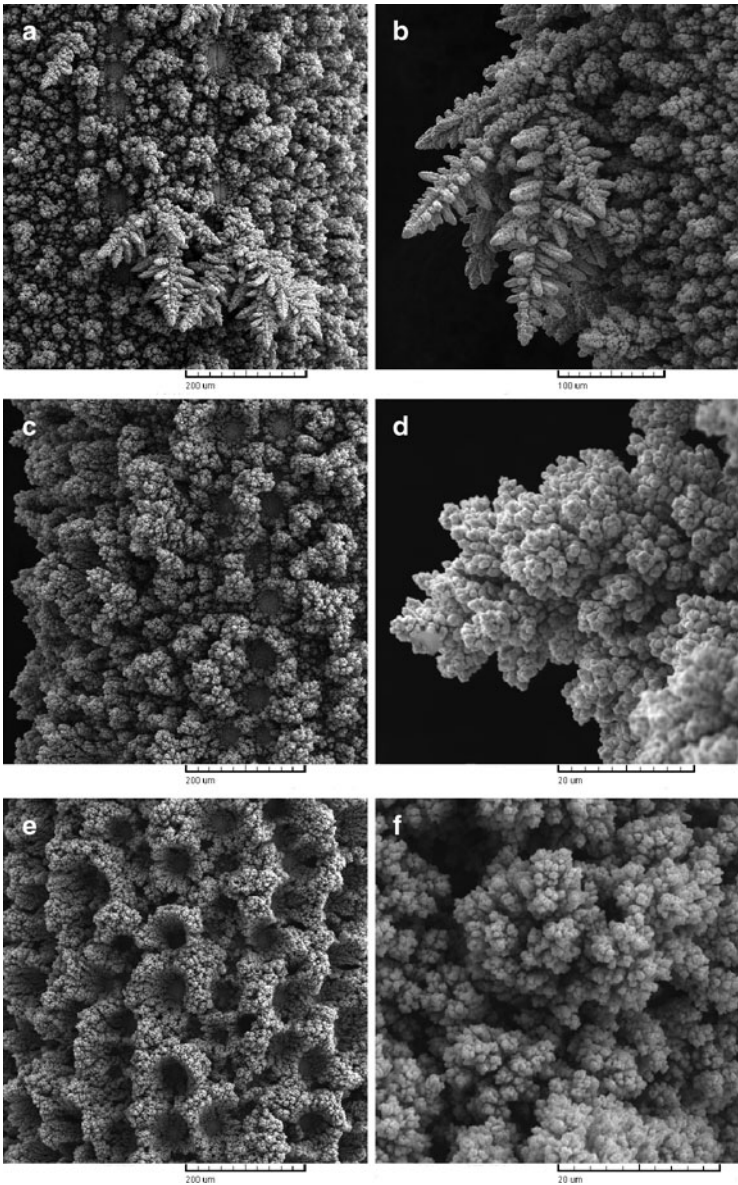
Fig. 3.5 Copper deposits obtained by the PC regimes with pause duration of 10 ms and deposition pulses of (**a**) and (**b**) 1 ms; (**c**) and (**d**) 2 ms; and (**e**) and (**f**) 50 ms (Reprinted from [47] with permission from Elsevier.)
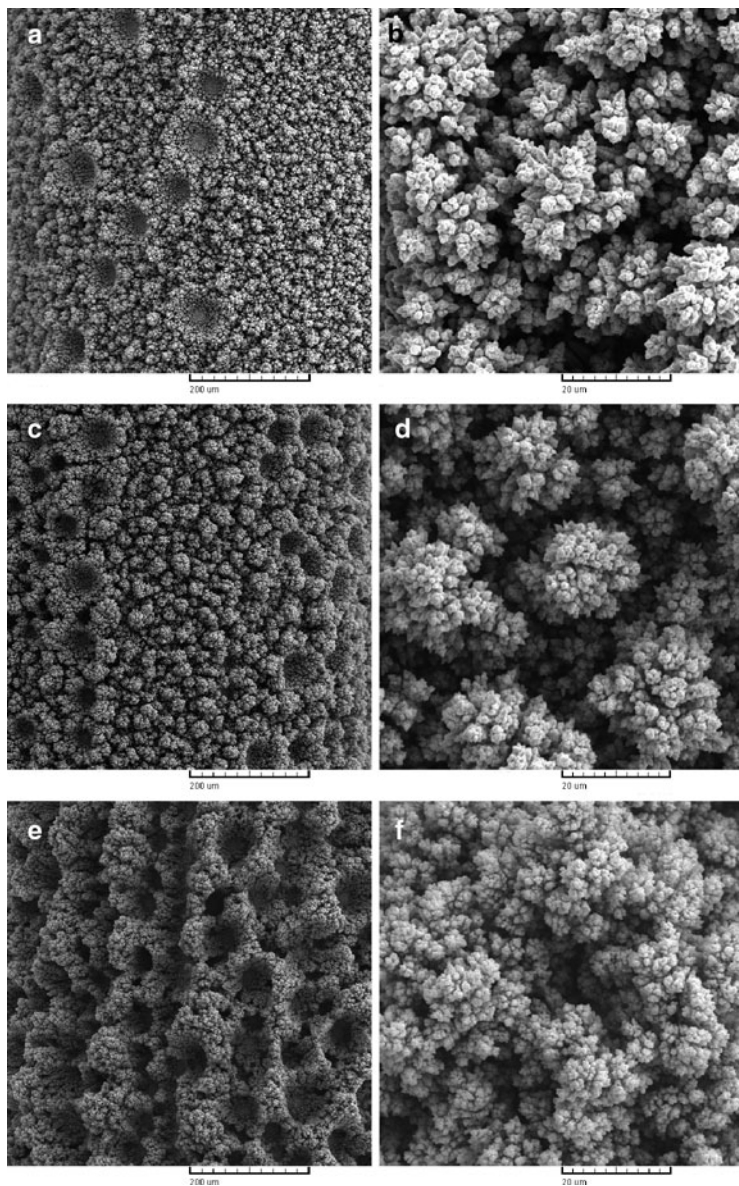
Fig. 3.6 Copper deposits obtained by the PC regimes with a deposition pulse of 10 ms and pause durations of (**a**) and (**b**) 100 ms; (**c**) and (**d**) 50 ms; and (**e**) and (**f**) 2 ms (Reprinted from [47] with permission from Elsevier.)

The selected parameters of square-wave PC enabled a comparison of the obtained morphologies of electrodeposited copper with those obtained by electrodepositions in the hydrogen codeposition range at the constant overpotential from six solutions of different concentrations of $CuSO_4$ and H_2SO_4 (see Figs. 3.3 and 3.4) [39]. It is clear that the effect of increasing concentration of Cu(II) ions was equivalent to the effect of the decreasing deposition pulses, while the constant pause duration was equivalent to H_2SO_4 concentration used. In a similar way, the effect of different H_2SO_4 concentrations (for the constant $CuSO_4$ concentration) can be correlated with the effect of different pause durations. The effect of increasing H_2SO_4 concentration was equivalent to the effect of decreasing the pause duration, while the constant $CuSO_4$ concentration is equivalent to the constant deposition pulse used [47]. Of course, the constant overpotential used corresponds to the amplitude current density used [47].

Hence, effects attained by the choice of appropriate parameters of square-wave PC were equivalent to those obtained by electrodeposition at the constant overpotential in the hydrogen codeposition range from solutions of different concentrations of $CuSO_4$ and H_2SO_4. In this way, the ionic equilibrium in the $CuSO_4$–H_2SO_4–H_2O system, determined by the dependence of the relative concentration of H^+ ions on H_2SO_4 concentration for different copper concentration, was successfully simulated. Also, the substitution of more different electrodeposition solutions by the one solution was achieved. This is of potential high technological significance because it enables saving of chemicals for the preparation of electrodeposition baths, as well as saving of place in the plating plants due to the reduced number of needed electrochemical cells.

The presented disperse or irregular morphological forms of copper may be useful in the production of powders [6, 32], while the honeycomb-like deposit type is due to an open porous structure with the extremely high surface area ideally suited to be used as electrodes in many electrochemical devices, such as fuel cells, batteries, and sensors [48].

It is easy to use the pulsating overpotential in laboratory-scale cells, but difficulties arise on a practical scale because of the demands for higher power and a high-speed potentiostat. It is easier to obtain pulsating or reversing currents on a practical scale, and, because of

this, the deposition of metal powders with the desired properties obtained by pulsating and reversing currents is of greater practical importance than that obtained by the pulsating overpotential.

3.3 Copper Powder Particles

3.3.1 Basic Facts

Pure copper powder is used in the electrical and the electronics industries because of its excellent electrical and thermal conductivities [49]. Alloyed with tin, zinc, nickel, and other elements, copper in powder form is used in structural parts and friction materials. Brasses, bronzes, and other copper alloys produced by powder metallurgy methods have the physical and mechanical properties of their cast or wrought counterparts. Copper is also used as an alloying element in iron powder components to enhance the mechanical properties and control dimensional changes during sintering, the addition being made either by mixing or by infiltration.

Probably the best known application of copper powder is the self-lubricating bearing which was the first major application and still accounts for about 70% of the granular copper powder used. This application takes advantage of the ability to produce a component with controlled interconnected and surface-connected porosity. The production of metallic filters also takes advantage of this ability.

In addition to the above applications of granular copper powder, a large quantity of copper and copper alloy powder is used in flake form, i.e., as a powder whose thickness is small in relation to its other dimensions. Such powders are used, for example, in antifouling paints, decorative and protective coatings, and printing inks.

Copper and copper alloy powders are also used in such nonstructural applications as brazing, cold soldering, and mechanical plating, as well as for medals and medallions, metal–plastic decorative products, and a variety of chemical and medical purposes.

Due to the ionic equilibrium of species in the $CuSO_4$–H_2SO_4–H_2O system, the formation of copper powder particles by electrolytic

technique is closely related to the quantity of hydrogen generated at the cathode surface during electrolysis. The shape and size of electrolitically formed powder particles strongly depend on concentrations of deposition ion and supporting electrolyte (that are $CuSO_4$ and H_2SO_4 concentrations for acid sulfate solutions), temperature of electrolysis, the applied current density or overpotential of electrodeposition, as well as of the time of removal of powder from the electrode surface, the type of working electrode used, rotation speed of cathode, and electrolyte circulation rate [4, 6, 50–53].

On the other hand, due to the fact that morphology of a deposit is determined by overpotential of electrodeposition, the structure of powder particles will not depend on electrolysis time in the potentiostatic conditions of electrodeposition. In the galvanostatic regime of electrolysis, overpotential of electrodeposition changes with electrolysis time, and for that reason, this regime of electrolysis is not suitable for basic experiments required for a theoretical consideration.

3.3.2   Correlation Between Morphology of Powder Particles Obtained by the Different Regimes of Electrolysis and the Quantity of Evolved Hydrogen

3.3.2.1   Morphologies of Powdered Deposits and Powder Particles Obtained by the Constant Potentiostatic Regime

In the dependence of the quantity of evolved hydrogen, the two types of powdered deposits are formed [32, 54]. The typical powdered deposits electrodeposited from 0.075 M $CuSO_4$ in 0.50 M H_2SO_4 at an overpotential of 650 mV (plateau of the limiting diffusion current density) and at an overpotential of 1,000 mV (about 250 mV above the plateau) are shown in Fig. 3.7a, b, respectively.

Very branchy dendrites and cauliflower-like agglomerates of copper grains were formed during electrodeposition at an overpotential of 650 mV (Fig. 3.7a). The amount of hydrogen evolved
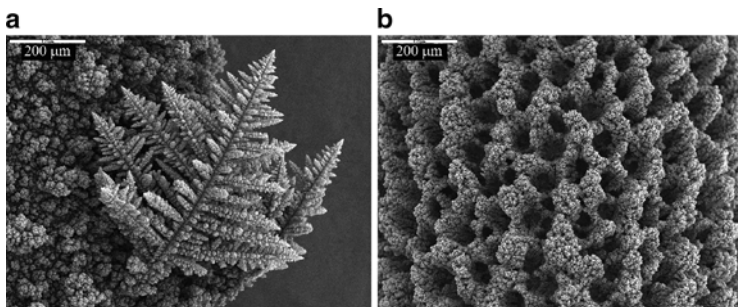
Fig. 3.7 Macrostructures of copper powdered deposits electrodeposited at overpotentials of: (**a**) 650 mV and (**b**) 1,000 mV (Reprinted from [54] with permission from Electrochemical Society.)

for the formation of this deposit type corresponds to an average current efficiency of hydrogen evolution of 7.5% [31], and it was below the critical value for the change of hydrodynamic conditions in the near-electrode layer [31]. The electrodeposition, where the formation of highly branched dendrites takes place, is rather diffusion than electron transfer controlled process [5].

The second type of powdered deposits is formed by electrodeposition at an overpotential of 1,000 mV (Fig. 3.7b). As expected, it is a typical honeycomb-like structure composed of holes formed by attached hydrogen bubbles and cauliflower-like agglomerates of copper grains formed around them. An average current efficiency of hydrogen evolution of 68.7% for this case was reported [42], and it was above the critical value for the change of hydrodynamic conditions in the near-electrode layer. The amount of evolved hydrogen was enough to cause effective solution stirring in the near-electrode layer leading to a decrease of the cathode diffusion layer thickness and to an increase of the limiting diffusion current density [30].

The dendritic particle obtained by tapping of the copper deposit presented in Fig. 3.7a is shown in Fig. 3.8a. The dendritic character of this particle is made of the corncob-like elements as shown in Fig. 3.8b. The ultrasonic treatment of copper dendrites showed that the corncob-like forms were the basic elements of which copper dendrites are composed [32]. A further analysis of the corncob-like
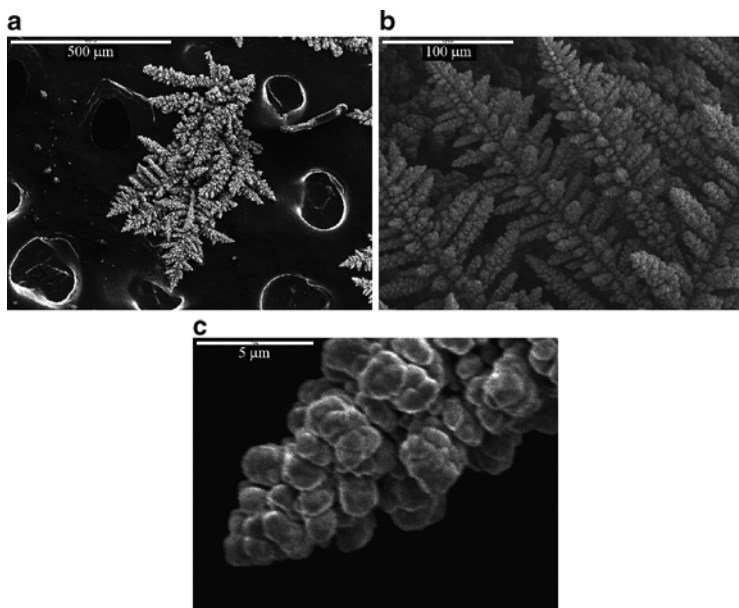
Fig. 3.8 (**a**) Dendritic particle obtained by tapping of the copper deposit electrodeposited at an overpotential of 650 mV, (**b**) corncob-like elements of which dendrites are composed; and (**c**) microstructure of the corncob-like element (Reprinted from [54] with permission from Electrochemical Society.)

elements at the microlevel found that they are composed of small agglomerates of copper grains (Fig. 3.8c).

In the dependence of concentration of Cu(II) ions, and hence the quantity of evolved hydrogen, the corncob-like elements can be grouped the different forms of dendritic particles from tree-like to those formed as flowers (Fig. 3.9a, b) or alternatively can be formed individually at the electrode surface (Fig. 3.9c) [31].

A particle obtained by tapping of the copper deposit electrodeposited at an overpotential of 1,000 mV is shown in Fig. 3.10a. Channel structure generated through the interior of the particle by the simultaneous copper nucleation and strong hydrogen evolution *in situ* can easily be seen from Fig. 3.10a. This type of powder consists of an aggregate of small cauliflower-like particles (Fig. 3.10b). Top view of the powder shown in Fig. 3.10a clearly revealed its
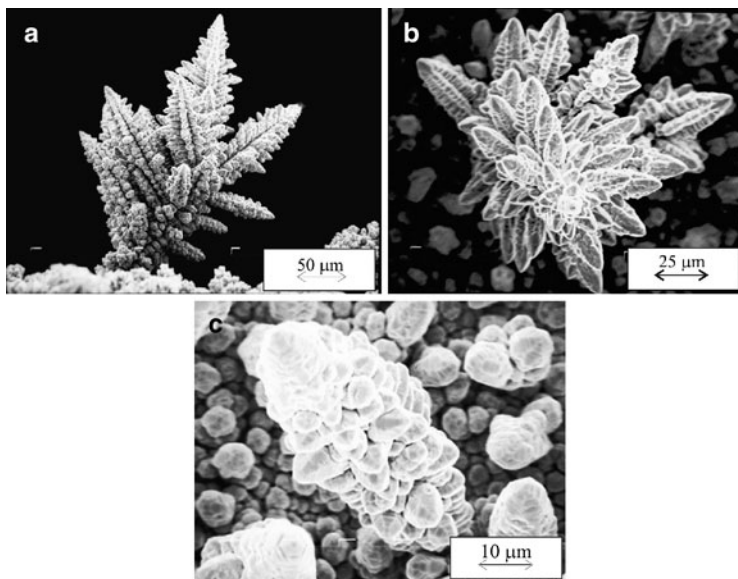
Fig. 3.9 Copper dendrites electrodeposited at an overpotential of 650 mV from (**a**) 0.075 M, (**b**) 0.30 M; and (**c**) 0.60 M CuSO$_4$ in 0.50 M H$_2$SO$_4$ (Reprinted from [32] with permission from Elsevier and [38] with permission from Springer.)

cauliflower-like character (Fig. 3.10c). An analysis of the cauliflower-like forms at the microlevel showed that they were composed of small agglomerates of copper grains (Fig. 3.10d). When this powder was ultrasonically treated the results showed that the basic element of these particles has the shape of a degenerate dendrite [32].

Anyway, the macrostructure of the formed powdered deposits was very different (Fig. 3.7). On the other hand, the similarity of the deposits at the microlevel is evident (Figs. 3.8c and 3.10d). The obvious difference is in the size of the individual copper grains of which the particles are comprised. The smaller size of the individual copper grains produced at an overpotential of 1,000 mV in comparison with the size of those deposited at 650 mV is attributable to the higher nucleation rate at an increased overpotential.
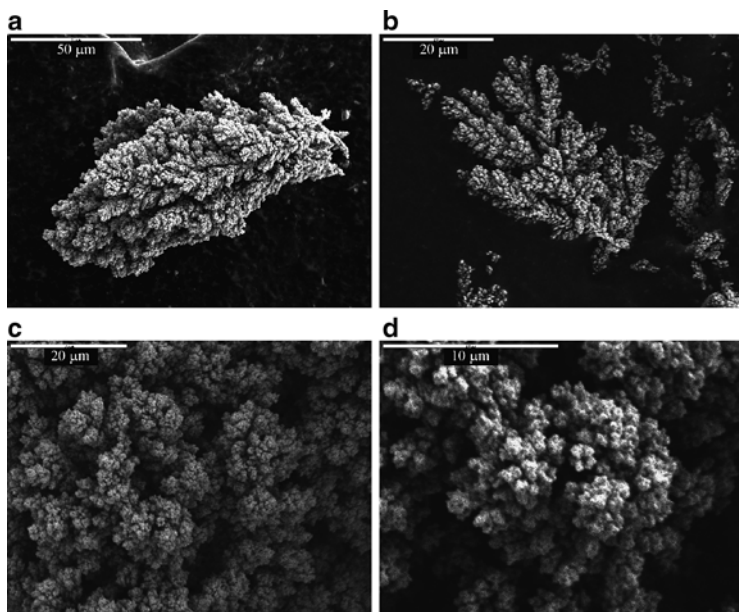
Fig. 3.10 (**a**) Powder particle obtained by tapping of the copper deposit electro-deposited at an overpotential of 1,000 mV, (**b**) and (**c**) cauliflower-like character of this type of the powder particle, and (**d**) microstructure of the cauliflower-like particle (Reprinted from [54] with permission from Electrochemical Society.)

The special case was the formation of powder by electrolysis from 0.30 M CuSO$_4$ in 0.50 M H$_2$SO$_4$ at an overpotential of 1,000 mV. This solution was denoted as transitional one between solutions with higher and lower concentrations of Cu(II) ions (in 0.50 M H$_2$SO$_4$) [42]. This deposit (Fig. 3.11a) contains characteristic of both types of powdered deposits: holes formed by attached hydrogen bubbles (Fig. 3.11a) and very branchy dendrites formed around them (Fig. 3.11b, c) [55]. The amount of evolved hydrogen spent for the formation of this deposit corresponded to the average current efficiency of hydrogen evolution of 16.0% [42]. The typical dendritic particle obtained by the tapping of this deposit is shown in Fig. 3.11d.
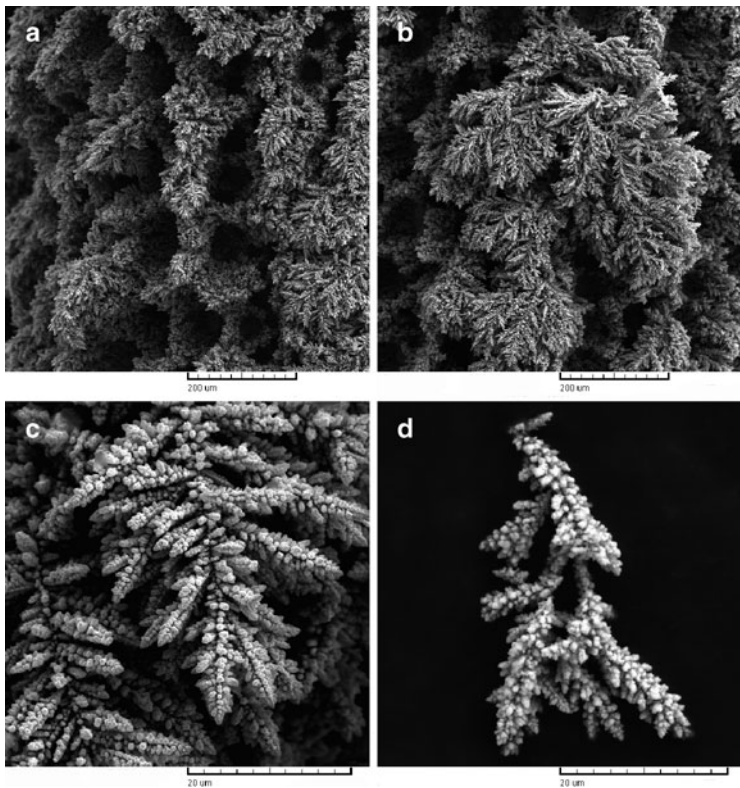
Fig. 3.11 Morphology of the copper deposit obtained by electrodeposition from 0.30 M $CuSO_4$ in 0.50 M H_2SO_4 at an overpotential of 1,000 mV: (**a**) top view, (**b**) and (**c**) magnified parts from (**a**); and (**d**) dendritic particle obtained by the tapping of the powdered deposit shown in (**a**)

3.3.2.2 Morphologies of Powdered Deposits and Powder Particles Obtained by the Regime of Pulsating Overpotential

Figure 3.12a, b shows the honeycomb-like structures electrodeposited from 0.15 M $CuSO_4$ in 0.50 M H_2SO_4 by the regimes of pulsating overpotential (PO) with the overpotential amplitude of 1,000 mV, a pause duration of 10 ms, and deposition pulses of 3 ms (Fig. 3.12a) and
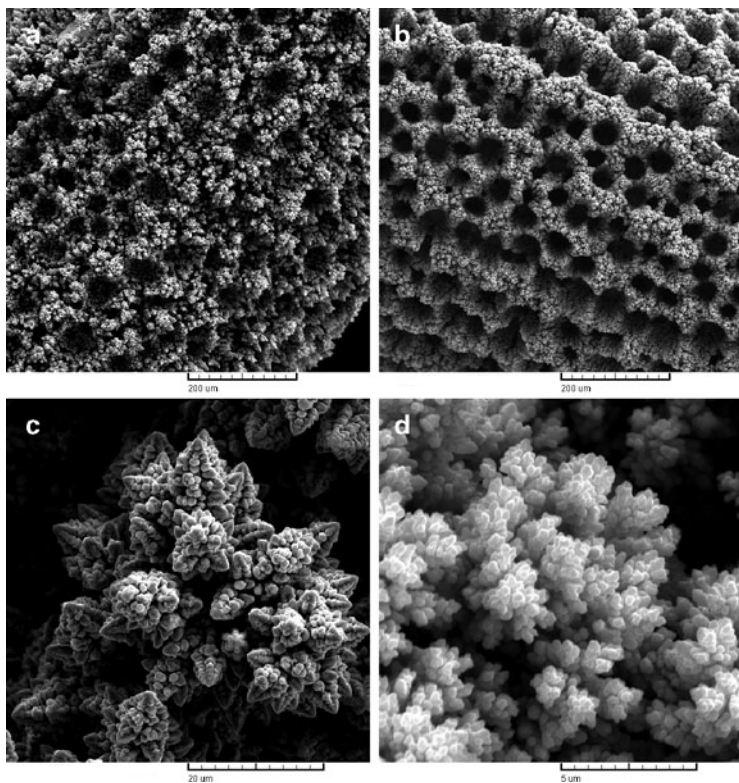
Fig. 3.12 Powdered deposits electrodeposited by the pulsating overpotential (PO) regime with a deposition pulse of (**a**) 3 ms, (**b**) 20 ms, (**c**) magnified part from (**a**), and (**d**) magnified part from (**b**). Pause duration: 10 ms. Overpotential amplitude: 1,000 mV. Solution: 0.15 M $CuSO_4$ in 0.50 M H_2SO_4

20 ms (Fig. 3.12b). Electrodepositions were performed at the room temperature using cylindrical copper wires as working electrodes. The amount of hydrogen generated during the formation of these powdered deposits corresponded to the average current efficiencies of hydrogen evolution of 16.4% for a deposition pulse of 3 ms and 28.1% for a deposition pulse of 20 ms [56]. The increased details from Fig. 3.12a, b which reveal the surface morphology around holes are shown in Fig. 3.12c, d, respectively. Very branchy dendrites are formed
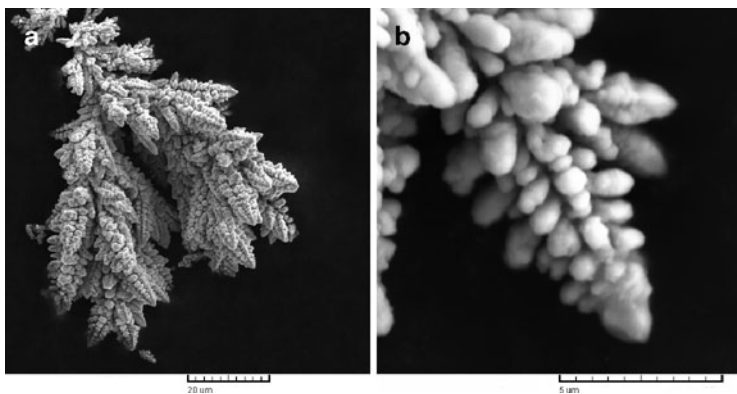
Fig. 3.13 Dendritic particle obtained by tapping of the powdered deposit electrodeposited by the pulsating overpotential (PO) regime with a deposition pulse of 3 ms (**a**) top view and (**b**) magnified part from (**a**). Pause duration: 10 ms. Overpotential amplitude: 1,000 mV. Solution: 0.15 M $CuSO_4$ in 0.50 M H_2SO_4

with a deposition pulse of 3 ms (Fig. 3.12c), while cauliflower-like agglomerates of copper grains were formed with a deposition pulse of 20 ms (Fig. 3.12d).

Dendritic particle obtained by tapping of the powdered deposit obtained with a deposition pulse of 3 ms is shown in Fig. 3.13a. Copper dendrites are constructed from corncob-like elements. Micro-analysis of corncob-like elements revealed that they are composed of small agglomerates of copper grains (Fig. 3.13b).

The SEM micrograph of the particle obtained by tapping of the powdered deposit obtained with a deposition pulse of 20 ms is shown in Fig. 3.14a. A channel structure formed by *in situ* by the simulta-neous processes of copper nucleation and strong hydrogen evolution can be easily noticed in this structure. Analysis of this particle at the higher magnification (Fig. 3.14b) showed that the particle is constructed from aggregates of small cauliflower-like agglomerates of copper grains.

Hence, the applied parameters of square-waves PO strongly affected hydrogen evolution reaction and hence morphology of cop-per powder particles. At the first sight, the effect of the shortening of deposition pulse duration was equivalent to the decrease of the
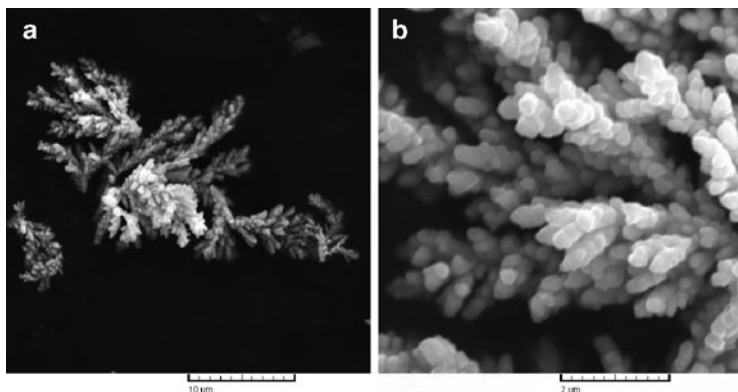
Fig. 3.14 Cauliflower-like particle obtained by tapping of the powdered deposit electrodeposited by the pulsating overpotential (PO) regime with a deposition pulse of 20 ms (**a**) top view and (**b**) magnified part from (**a**). Pause duration: 10 ms. Overpotential amplitude: 1,000 mV. Solution: 0.15 M $CuSO_4$ in 0.50 M H_2SO_4

overpotential of electrodeposition in the potentiostatic regime of electrolysis [32, 54]. It was shown [32, 54] that very branchy dendrites were electrodeposited from the same solution at overpotentials of 650 mV (Fig. 3.7a) [54] or 700 mV [32, 38], while aggregates of small cauliflower-like particles were obtained at an overpotential of 1,000 mV [32, 38].

3.3.2.3 Comparison of Morphologies of Powdered Deposits and Powder Particles Obtained by the Constant Potentiostatic Regime and by the Regime of Pulsating Overpotential

Considering the strong effect of parameters of the PO regime on both hydrogen evolution reaction and copper electrodeposition rate (Figs. 3.12–3.14), equivalence between morphology of copper powder particles obtained by the regime of PO and those obtained by electrodeposition in the potentiostatic regime from solutions of different concentrations of $CuSO_4$ and H_2SO_4 can be made and presented in the following way.

From Figs. 3.11 and 3.12, it is very clear that macromorphologies of deposits electrodeposited from 0.30 M $CuSO_4$ in 0.50 M H_2SO_4 at 1,000 mV and by the PO regime with a deposition pulse of 3 ms were very similar to each other; in both cases, holes formed by attached hydrogen bubbles surrounded by very branchy dendrites were formed.

It is necessary to note that both the powdered deposits were formed with approximately the same average current efficiency of hydrogen evolution ($\eta_{I,av}(H_2)$ of 16.0% for the deposit obtained in the potentiostatic deposition and $\eta_{I,av}(H_2)$ of 16.4% for the deposit obtained by square-wave PO with a deposition pulse of 3 ms).

In the PO regimes, the average current efficiency for hydrogen evolution reaction increases with the prolongation of deposition pulse duration approaching to the one obtained at the constant over-potential [56]. Then, copper electrodeposition from 0.15 M $CuSO_4$ in 0.50 M H_2SO_4 by the PO regime with a deposition pulse of 20 ms ($\eta_{I,av}(H_2) = 28.1\%$) should compare with the one from the same solution at an overpotential of 1,000 mV ($\eta_{I,av}(H_2) = 30.0\%$). Meanwhile, having in view the fact that macrostructures of the honeycomb-like deposits obtained with the average current efficencies of hydrogen evolution of 30.0% and with higher ones were consisted of holes formed by attached hydrogen bubbles and cauli-flower-like agglomerates of copper grains around them [38], powder particles formed with a deposition pulse of 20 ms can be compared with those formed by electrodeposition from 0.075 M $CuSO_4$ in 0.50 H_2SO_4 at an overpotential of 1,000 mV (Figs. 3.7b and 3.10). In both cases, particles composed of small cauliflower-like agglo-merates of copper grains were formed.

Comparing morphologies of powder particles (as well as the powdered deposits) obtained by the PO regimes with the different length of deposition pulse with those obtained by electrodeposition in the potentiostatic regime at 1,000 mV from solutions of different concentrations of $CuSO_4$ and H_2SO_4, it is clear that effect of the increase of deposition pulse duration on both hydrogen evolution reaction and copper electrodeposition rate was equivalent to the one observed by the decrease of $CuSO_4$ concentration (for the constant H_2SO_4 concentration). The effect of the constant pause duration ($t_p = 10$ ms) was equivalent to the constant H_2SO_4 concentration.

Of course, the overpotential amplitude in the PO regimes corresponded to the overpotential of electrodeposition in the constant regimes of electrolysis.

3.3.2.4 General Discussion

In the dependence of solution composition, regime of electrolysis and preparing of the working electrode, the copper surface morphologies can be grouped into the three hydrogen codeposition range:

(I) The range of the average current efficiencies of hydrogen evolution, $\eta_{I,av}(H_2)$, between 0 and 10.0%—the dominant presence of branchy dendrites, independently formed cauliflower-like forms, and the possible formation of individual holes of detached hydrogen bubbles (dish-like hole) [30, 31, 38, 41].

(II) The range of the average current efficiencies of hydrogen evolution, $\eta_{I,av}(H_2)$, between 10.0 and 20.0%—the mixture of dish-like holes and holes constructing the honeycomb-like structure with independently formed copper grains agglomerates among them [42], as well as the mixtures of holes and cauliflower-like forms [30, 38], and holes and branchy dendrites (Figs. 3.11a and 3.12a).

(III) With $\eta_{I,av}(H_2)$ above 20.0%—the mixture of holes and cauliflower-like copper grains agglomerates formed around holes without the appearing of dendrites [30, 31, 38, 41, 42].

In general, the number of holes increased with intensification of hydrogen evolution reaction while the shape of holes changed from dish-like holes to holes constructing the honeycomb-like structure. The honeycomb-like structures are formed with $\eta_{I,av}(H_2)$ larger than 10.0% [30, 38]. The quantity of the evolved hydrogen corresponding to the average current efficiency of hydrogen evolution, $\eta_{I,av}(H_2)$, of 10.0% was just denoted as the critical quantity leading to the formation of the honeycomb-like structures [31]. This critical quantity of generated hydrogen is mostly spent for the creating of holes in the honeycomb-like type of structure and it does not cause a stirring of the solution, and hence it does not affect hydrodynamic conditions in the near-electrode layer. On the other hand, with the increasing

quantity of evolved hydrogen, the change of surface morphology from dendrites to cauliflower-like agglomerates of copper grains formed around holes was observed.

The analysis of the copper surface morphologies classified in all three hydrogen codeposition ranges indicates that the overall quantity of evolved hydrogen can be divided into two parts. The one part of evolved hydrogen is spent for the creating of holes and their increase with electrolysis time, while the other part of evolved hydrogen (or the rest of the overall quantity of evolved hydrogen) determines morphology of deposits. This can be explained as follows.

In the initial stage of electrodeposition, both hydrogen evolution and copper nucleation occur at the most active energy sites of the electrode surface [38, 57]. The formed hydrogen bubbles isolate substrate and current lines are concentrated around them forming rings composed of agglomerates of copper grains. Simultaneously, small agglomerates of copper grains are formed at the electrode surface of copper nucleus formed in the initial stage of electrodeposition among hydrogen bubbles. In the growth process, due to the effect of current density distribution, further copper nucleation and hydrogen evolution primarily occur at top of both groups of copper grains agglomerates. Some of new, freshly formed hydrogen bubbles will coalesce with hydrogen bubbles formed in the initial stage of electrodeposition leading to their growth with electrolysis time. When the critical size of these hydrogen bubbles to detach from the electrode surface is attained, they will detach forming holes at the electrode surface. This quantity of evolved hydrogen does not contribute to stirring of solution and to the change of hydrodynamic conditions in the near-electrode layer.

Meanwhile, some of new, freshly formed hydrogen bubbles at the top of agglomerates around initially formed hydrogen bubbles will not coalesce with them, because they are situated between freshly formed copper nuclei which represent barrier to find a path and to coalesce with initially formed hydrogen bubbles. Also, they cannot develop in large hydrogen bubbles for the same reasons. The similar situation occurs at top of those copper grains agglomerates which are formed of initially formed copper nuclei. These hydrogen bubbles will detach from the electrode surface very fast forming "current of hydrogen" which cause stirring of the solution and strongly affect

hydrodynamic conditions in the near-electrode layer. Morphology of copper deposits is determined by this quantity of evolved hydrogen.

The fact that morphology of electrodeposited copper is determined by the difference between the overall quantity of evolved hydrogen and those spent for the creating of holes can be confirmed by the following consideration.

As already mentioned, the following disperse copper structures were formed in the range of $\eta_{I,av}(H_2)$ between 10.0 and 20.0% (group (II)): the mixture of dish-like holes and holes constructing the honeycomb-like structure [42], as well as the honeycomb-like structures constructed from holes surrounded by relatively compact cauliflower-like agglomerates of copper grains ($\eta_{I,av}(H_2) = 10.8\%$) [30] or branchy dendrites (Figs. 3.11a and 3.12a). Making the difference between the overall quantity of evolved hydrogen and the critical quantity of evolved hydrogen spent for the formation of the honeycomb-like structures ($\eta_{I,av}(H_2)$ of 10.0%), the excellent agreement between the morphological forms obtained in this hydrogen codeposition range and those obtained in the hydrogen codeposition range between 0 and 10.0% was observed. Very compact copper grains cauliflower-like agglomerates, branchy dendrites, and individual dish-like holes are obtained with a quantity of evolved hydrogen in the range of the average current efficiencies of hydrogen evolution between 0 and 10.0%. The diffusion layer of the macroelectrode was not disturbed by the formation of these morphological forms indicating that these quantities of evolved hydrogen are insufficient to cause the solution stirring and to the change of hydrodynamic conditions in the near-electrode layer.

Meanwhile, dendrites are not formed by electrodeposition processes accompanied by $\eta_{I,av}(H_2)$ larger than 20.0%. Honeycomb-like structures consisted of holes and very disperse cauliflower-like agglomerates of copper grains were formed by these electrodeposition processes [38]. The difference between the overall quantity of evolved hydrogen and the critical value for the creating of holes in the honeycomb-like ones gives the effective quantity of evolved hydrogen larger than 10.0%. This quantity of evolved hydrogen was sufficient to cause effective solution stirring leading to the change of hydrodynamic conditions in the near-electrode layer.

3.4 Analysis of Decisive Properties of Powders

As stated in Introduction, some properties, called the decisive properties, characterize the behavior of metal powder. The most important of them are the specific surface, the apparent density, the flowability, the particle grain size, and the particle size distribution [1]. These properties were analyzed by Popov et al. [58–73] which showed that some of them can be mutually related, as well as that the specific surface of copper powder can be related to the overpotential of electrodeposition [58, 59].

3.4.1 Correlation Between Specific Surface and Overpotential of Electrodeposition

The specific surface of a powder and a powdered deposit is determined as the surface per unit of the mass of powder.

It is well known [74, 75] that the surface coarseness during potentiostatic electrodeposition in the mixed activation–diffusion control increases with the increase of the current density of electrodeposition. The surface coarseness also increases during potentiostatic electrodeposition at the limiting diffusion current density with an increase of overpotential [18, 76], resulting in the formation of dendrites. In metal electrodeposition in the limiting diffusion current density range, the real current density remains constant regardless of the overpotential used. Simultaneously, the larger overpotential of electrodeposition is used, the more disperse deposit characterized by the increased specific surface is formed.

The last effect can be qualitatively discussed as follows.

The overpotential of electrodeposition, η, in the region of mixed activation–diffusion control is given by Eq. (3.19):

$$\eta = \frac{b_{\mathrm{c}}}{2.3} \ln \frac{j}{j_0} + \frac{b_{\mathrm{c}}}{2.3} \ln \frac{1}{1 - \frac{j}{j_{\mathrm{L}}}}. \tag{3.19}$$

The activation part of electrodeposition overpotential required for the charge transfer, η_{act}, is given by Eq. (3.20):

$$\eta_{act} = \frac{b_c}{2.3} \ln \frac{j}{j_0} \qquad (3.20)$$

and the rest of the overpotential, η_{diff}, given by Eq. (3.21) is due to mass transfer limitations:

$$\eta_{diff} = \frac{b_c}{2.3} \ln \frac{1}{1 - \frac{j}{j_L}}. \qquad (3.21)$$

Hence, if $j \to j_L$,

$$\eta_{act} = \frac{b_c}{2.3} \ln \frac{j_L}{j_0}, \qquad (3.22)$$

being equal to the critical overpotential for the initiation of dendritic growth [5, 27]. Simultaneously, for $j \to j_L$

$$\eta_{diff} \to \infty. \qquad (3.23)$$

It is obvious that a very small increase of current density in the limiting diffusion current density range causes a large increase in deposition overpotential. Hence, the charge transfer overpotential and the ohmic drop in the solution remain the same for all overpotentials belonging to the limiting diffusion current density plateau, regardless of electrodeposition overpotential. This is due to the fact that both the charge transfer overpotential and the ohmic drop only depend on the current density. On the other hand, an increase of the deposition overpotential in the limiting diffusion current density range causes a strong increase of the dispersity and hence an increase of the specific surface area of metal deposits. Hence, it seems reasonable to assume that the difference in overpotential of electrodeposition can be related to the increase of the specific surface of the deposited metal by the relation [58, 59]

$$\gamma(S_2 - S_1) = (\eta_2 - \eta_1) \int_0^t I \mathrm{d}t, \tag{3.24}$$

where I is a current of electrodeposition, t is a time of electrode-position, $\int_0^t I \mathrm{d}t$ is the quantity of passed electricity, η_2 and η_1 are overpotentials of electrodeposition belonging to the limiting diffusion current density range, S_2 and S_1 are the surface area of disperse deposits at the overpotentials η_2 and η_1, respectively, and γ is the surface energy of disperse deposit formation.

Equation (3.24) can be rewritten in the form

$$\gamma = \frac{(\eta_2 - \eta_1) \int_0^t I \mathrm{d}t}{(S_2 - S_1)} \tag{3.25}$$

for the direct determination of the energy of disperse solid copper surface formation in sulfate solutions.

The energy of disperse solid copper surface formation, γ, calculated by Eq. (3.25) includes all energetic loss during electrodeposition in the range of the limiting diffusion current densities.

For the estimation of the surface energy of disperse deposits formation, γ, according to Eq. (3.25), it is necessary to determine surface area of deposits, S_2 and S_1, at overpotentials η_2 and η_1 belonging to the limiting diffusion current density range. Obviously, the surface area of a deposit S_1 corresponds to an overpotential η_1 at the beginning of the limiting diffusion current density plateau, while the surface area of a deposit S_2 corresponds to an overpotential η_2 at the end of the limiting diffusion current density plateau. During the depositions, I–t dependences were recorded and the quantity of electricity, $\int_0^t I \mathrm{d}t$ was determined by a graphical integration.

Due to very high surface areas of powdered (or disperse) deposits, the determination of real surface area of this deposit type can represent serious problem [71]. The determination of the real surface area of disperse metal deposits by some common methods, such as the use of STM and AFM techniques (using the option surface area diff., in the accompanying software package), is not possible, because these techniques are suitable for the determination of the real surface area of only compact and relatively smooth surface area [77, 78].

For that reason, the new and relatively easy way for the estimation of the real surface area of disperse deposits was proposed by Popov et al. [58, 59, 71]. For copper solution containing 0.15 M $CuSO_4$ in 0.50 M H_2SO_4, this estimation can be presented in the following way: working electrode (copper or platinum) of surface area $S_{0,i}$ is covered by a thin copper film by electrodeposition at an overpotential of 300 mV during 2 min. After a relaxation of the diffusion layer for 15 min, current at an overpotential of 50 mV, I_0, is recorded, being proportional to the original electrode surface area $S_{0,i}$. The overpotential is then adjusted to the desired value, and electrode-position is carried out. After the determined quantity of electricity had been reached, the overpotential is decreased to 50 mV, and after relaxation of the diffusion layer for 15 min, the current I_η, corresponding to the surface area S_f generated during electrodeposition, is determined. The surface area of the deposit is then calculated using Eq. (3.26):

$$S_f = S_{0,i} \frac{I_\eta}{I_0} - S_{0,i} = S_{0,i} \left(\frac{I_\eta}{I_0} - 1 \right). \qquad (3.26)$$

It is well known [6] that dendrites are not formed at overpotentials of electrodeposition lower than a critical overpotential for dendritic growth initiation, η_i, and that powdered deposits characterized by a very large surface area are formed at overpotentials higher than some critical value η_c.

For $\eta_2 \geq \eta_c$, $\eta_1 \geq \eta_i$ and $S_2 >> S_1$, Eq. (3.25) can be rewritten in the form

$$S_2 = \frac{(\eta_2 - \eta_1) \int\limits_0^t I \mathrm{d}t}{\gamma}. \qquad (3.27)$$

On the other hand, the quantity of electrodeposited metal m is given by

$$m = \frac{M}{nF} \int\limits_0^t I \mathrm{d}t, \qquad (3.28)$$

assuming the current efficiency for metal electrodeposition $\eta_I(M)$ to be 1, where M is the atomic mass of deposited metal. From Eqs. (3.27) and (3.28), the specific powder (or powdered deposit) surface S_{sp} is

$$S_{sp} = \frac{S_2}{m} = \frac{(\eta_2 - \eta_1)nF}{\gamma M}. \qquad (3.29)$$

If the current efficiency for metal electrodeposition, $\eta_I(M)$, is lower than 1, Eq. (3.28) becomes

$$m = \eta_I(M) \frac{M}{nF} \int\limits_0^t I \mathrm{d}t \qquad (3.30)$$

and Eq. (3.29) becomes:

$$S_{sp} = \frac{(\eta_2 - \eta_1)nF}{\eta_I(M)\gamma M}. \qquad (3.31)$$

Equations (3.30) and (3.31) are valid in the hydrogen codeposition range at overpotentials lower than the critical one for the change of the growth of dendrites. The situation is dramatically different in galvanostatic electrodeposition of powder. In this case, due to the increase of the surface coarseness, the low increase of the limiting diffusion current density caused by the increase of the surface area of a deposit leads to the strong decrease of overpotential of the electrodeposition in the limiting diffusion current density range even with the short deposition times. The internal structure of powder particles does not change with time during potentiostatic electrodeposition, and it only depends on the presence or the absence of hydrogen codeposition. In the galvanostatic case, the structure of particles becomes a more compact with the increasing time of electrodeposition and it can be changed from dendrites at the beginning of the electrodeposition process to the compact one with the longer electrodeposition time, as shown in Fig. 3.15a (*Powder A*) [60, 66]. In the hydrogen codeposition range, the overpotential of electrodeposition is determined by hydrogen reduction and at sufficiently large initial
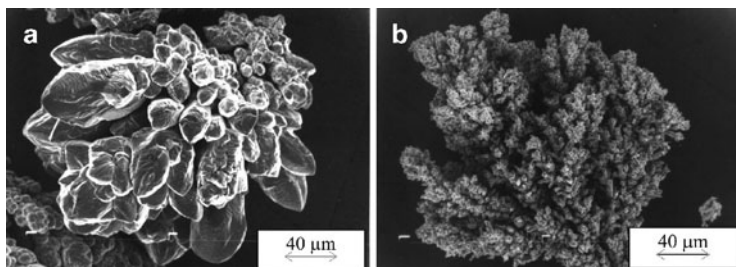
Fig. 3.15 SEM photomicrographs of copper powder particles obtained in constant current deposition. $c(Cu^{2+}) = 15$ g/dm^3, $c(H_2SO_4) = 140$ g/dm^3, $Q = 0.11$ dm^3/min^1, $t = (50\pm2)°C$, fraction (149–177) μm: (**a**) $j = 1,800$ A/m^2, $\tau_r = 1.5$ h, apparent density 1.122 g/cm^3 and (**b**) $j = 3,600$ A m^2, $\tau_r = 15$ min, apparent density 0.524 g/cm^3 (Reprinted from [60] with permission from NOVA publishers, [66] with permission from the Serbian Chemical Society and copied by permission from the "Electrochemistry Encyclopedia" (http://electrochem. cwru.edu/ed/encycl/) on 04/25/2007. The original material is subject to periodical changes and updates.)

current densities, $j \gg j_L$, as well as with enough short electrode-position times, the formation of copper powder in a galvanostatic deposition becomes similar to the one in potentiostatic electrodeposition, as shown in Fig. 3.15b (*Powder B*).

The described method for the determination of the specific surface of electrodeposited copper is applicable if some kind of a Faradaic cage is not formed on the surface of deposit, i.e., when the formed structure is "open" to the bulk of electrolyte solution in potentiostatic deposition.

According to Calusaru [3], the specific surface of copper powder is 500–3,000 cm^2 g^{-1} depending on the electrodeposition conditions. The critical overpotential for the dendritic growth initiation in copper sulfate acid solution is about 0.30 V, and the critical overpotential for the instantaneous dendritic growth initiation, which is equal to the critical overpotential of copper powder formation, is about 0.7 V [18]. Assuming that electrodeposition is carried out at an overpotential of the instantaneous dendritic growth initiation, we can show the following. Using the difference in the actual deposition overpotential and the overpotential corresponding to the beginning of the plateau of the limiting diffusion density as 0.40 V, γ determined in the presented

way as 2.7 J cm^{-2} [58, 59], and η_I(Cu) = 1, the minimum specific powder surface, S_{sp}, of 500 cm^2 g^{-1} is calculated, which is in good agreement with the findings of Calusaru [3].

If the electrodeposition overpotential and the overpotential of dendritic growth initiation from the examined electrolyte are known, it is obvious that the specific surface of copper powder can be calculated by Eq. (3.31) using this value of γ and the corresponding value of the current efficiency for copper electrodeposition. The upper limit of the value of the copper powder specific surface can be estimated as follows. Assuming that electrodeposition is carried out at 1.0 V with the current efficiency for copper electrodeposition of 0.5, $S_{sp} \cong$ 2,800 cm^2 g^{-1} is obtained using Eq. (3.31) which is in accordance with the data of Calusaru. In this way, one of the most important characteristics of copper powder is related to overpotential of the electrodeposition and hence to the electrodeposition conditions.

Also, the specific surface of powdered deposits can be related to morphology of deposits obtained at overpotentials belonging to the plateau of the limiting diffusion current density, as well as at the higher ones. This is presented by the analysis of copper electrodeposition processes from 0.15 M CuSO$_4$ in 0.50 M H$_2$SO$_4$ at overpotentials of 550 and 700 mV (the plateau of the limiting diffusion current density), as well as at overpotentials of 800 and 1,000 mV which are about 50 and 250 mV outside the plateau of the limiting diffusion current density [30, 38].

According to Eqs. (3.26), (3.30), and (3.31), the specific surface of the electrodeposited copper, $S_{sp,m}$, can be given by Eq. (3.32), where $\eta_I(M) = \eta_{I,av}(Cu)$:

$$S_{sp,m} = \frac{S_{0,i}\left(\frac{I_\eta}{I_0} - 1\right)}{\frac{\eta_{I,av}(Cu)\int_0^t I dt}{nF}M} = \frac{nFS_{0,i}}{\eta_{I,av}(Cu)M}\frac{1}{\int_0^t I dt}\left(\frac{I_\eta}{I_0} - 1\right). \qquad (3.32)$$

In this case, the number of electrons involved in the electrodeposition reaction, n, is 2, the atomic mass of copper, M, is 63.55 g mol^{-1}, and Faraday constant, F, is 96,485 As mol^{-1}. In this investigation, the original electrode surface before electrodeposition, $S_{0,i}$, was 0.50 cm^2.

Table 3.1 The average current efficiency for copper electrodeposition, $\eta_{I,av}(Cu)$ (%) obtained at different overpotentials

Overpotential, η (mV)	550	700	800	1,000
The average current efficiency for copper electrodeposition, $\eta_{I,av}(Cu)$ (%)	100	98.03	89.2	70.0
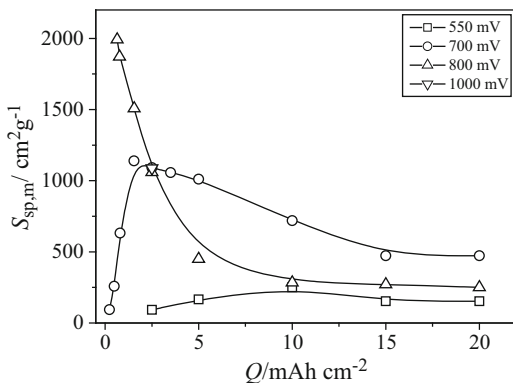
Fig. 3.16 The dependence of the specific surface of the electrodeposited copper on the quantity of the electricity, Q

Hydrogen evolution at an overpotential of 550 mV was not observed. The average current efficiencies of hydrogen evolution, $\eta_{I,av}(H_2)$ in %, at overpotentials of 700, 800, and 1,000 mV were 1.97, 10.8, and 30.0%, respectively [30, 38].

Since $\eta_{I,av}(Cu) + \eta_{I,av}(H_2) = 1$, the average current efficiencies for copper electrodeposition can be simply calculated and the obtained values are summarized in Table 3.1.

Current I_η and I_0 are obtained in an already described way.

Figure 3.16 shows the dependence of the specific surface of the electrodeposited copper on the quantity of the electricity. Two groups of the dependence of the specific surface of the electrodeposited copper on the quantity of the electricity are observed by the analysis of this figure.

In the first group are inserted the dependences of $S_{sp,m}$ on the quantity of the electricity Q obtained at overpotentials of 550 and 700 mV.
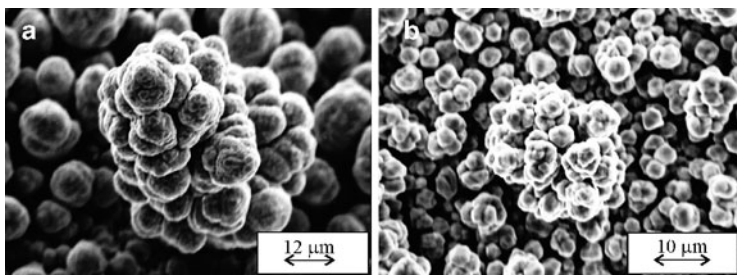
Fig. 3.17 Cauliflower-like forms electrodeposited at an overpotential of (**a**) 550 mV, quantity of the electricity: 10 mAh cm^{-2} and (**b**) 700 mV, quantity of the electricity: 2.5 mAh cm^{-2}
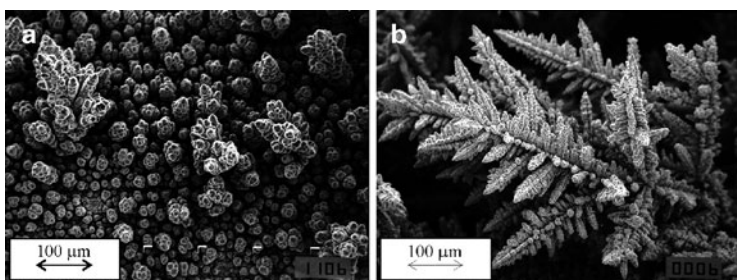

Fig. 3.18 Copper deposits obtained at an overpotential of (**a**) 550 mV; the quantity of the electricity: 20 mAh cm^{-2}, and (**b**) 700 mV; the quantity of the electricity: 10 mAh cm^{-2} (Reprinted from [79] with permission from Elsevier.)

At these overpotentials, there is no hydrogen evolution (550 mV) or it is very small (700 mV). The characteristic of this group is the existence of maximum of the specific surface at the determined quantity of the electricity. The increase of the overpotential led to the decrease of the quantity of the electricity needed to reach this maximum. The cauliflower-like forms, as those shown in Fig. 3.17, were obtained with a quantity of electricity of 10 and 2.5 mAh cm^{-2} at overpotentials of 550 and 700 mV, respectively.

The mixture of cauliflower-like forms and individual dendrites is formed at an overpotential of 550 mV with a quantity of electricity of 20 mAh cm^{-2} (Fig. 3.18a) [79], while very branchy copper dendrites (Fig. 3.18b) are formed at an overpotential of 700 mV with a quantity

of larger electricity of 2.5 mAh cm^{-2} [71]. Copper dendrites were consisted of corncob-like elements, and the whole electrode surfaces were covered with them after electrodeposition with quantities of the electricity larger (approximately 5.0 mAh cm^{-2}).

Anyway, the values of $S_{sp,m}$ obtained at an overpotential of 700 mV before initiation of dendritic growth, i.e., with the low quantities of passed electricity, are similar to those obtained at 550 mV with the larger quantities of electricity. The further increase of $S_{sp,m}$ with the increasing quantity of the electricity before dendritic growth initiation is due to the decrease of grain size of a deposit. After formation of both the precursors of dendrites and dendrites, $S_{sp,m}$ strongly increases and remains approximately constant up to the quantity of electricity at which the overlap of dendrites begins. With larger quantities of electricity, the $S_{sp,m}$ value decreases up to constant value which probably corresponds to the established front of dendrites growing to the bulk of the solution.

The second group of the dependences of $S_{sp,m}$ on Q is obtained at overpotentials of 800 and 1,000 mV. As already mentioned, at these overpotentials hydrogen evolution is vigorous enough to strongly affects hydrodynamic conditions in the near-electrode layer. From Fig. 3.16, it can be seen that there is no maximum of the specific surface in a function of quantity of the passed electricity. Due to the overlap of the agglomerates of grains during prolonged electrodeposition, the decrease of the specific surface of the electrodeposited copper with the increasing quantity of the electricity was observed. With the short electrodeposition times, $S_{sp,m}$ was very large. Also, it can be observed from Fig. 3.16 that there is not any difference between the specific surfaces obtained at overpotentials of 800 and 1,000 mV. SEM analysis of copper deposits obtained at these overpotentials showed that the honeycomb-like structures are formed at these overpotentials [30, 38]. The typical agglomerates of copper grains formed around holes are shown in Fig. 3.19. The decrease of grain size obtained at an overpotential of 1,000 mV in relation to those obtained at an overpotential of 800 mV is due to the increase of nucleation rate with the increase of overpotential. Anyway, copper dendrites were not formed during electrodepositions at overpotentials of 800 and 1,000 mV.

Figure 3.20 shows the dependence of the specific surface of the electrodeposited copper on overpotential of the electrodeposition for
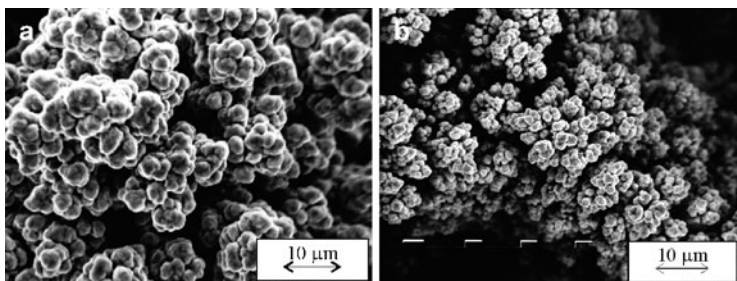
Fig. 3.19 Copper grain agglomerates obtained with the quantity of the electricity of 20 mAh cm^{-2} at an overpotential of (**a**) 800 mV, and (**b**) 1,000 mV
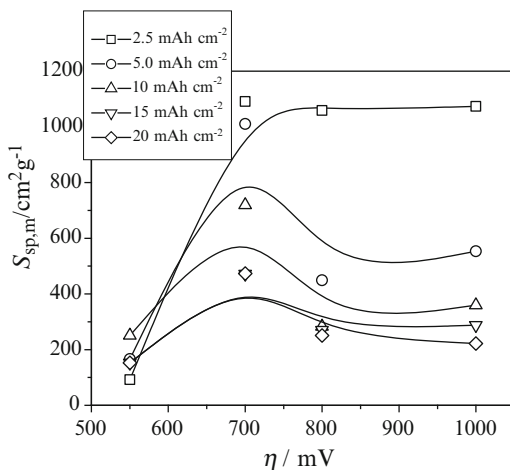

Fig. 3.20 The dependence of the specific surface of the electrodeposited copper on overpotential of the electrodeposition

different quantities of the electricity. Aside from for quantity of the electricity of 2.5 mAh cm^{-2}, the maximum of $S_{sp,m}$ is obtained at an overpotential of 700 mV with all the analyzed quantities of electricity. The formation of dendrites corresponds to these maximal values of $S_{sp,m}$.

The decrease of the specific surface with the increase of the overpotential of the electrodeposition from 700 to 800 mV can be

explained by the change of the hydrodynamic conditions in the near-electrode layer caused by hydrogen evolution. Due to the change of hydrodynamic conditions in the near-electrode layer, copper electrodeposition occurs at an overpotential which is effectively lower than the specified one. For that reason, morphologies of electrodeposited copper obtained at overpotentials of 800 and 1,000 mV are similar to ones obtained at some lower overpotentials before the initiation of dendritic growth (the concept of "effective overpotential") [30, 38].

The absence of maximum of the $S_{sp,m}$ for powdered deposits obtained with the quantity of the electricity of 2.5 mAh cm^{-2} can be explained by the fact that morphologies of copper deposits obtained with this quantity of the electricity did not depend on the overpotential used. The cauliflower-like agglomerates of copper grains were electrodeposited at all analyzed overpotentials.

Also, it is necessary to note that copper dendrites formed at overpotentials of 550 and 700 mV with the quantity of electricity of 20 mAh cm^{-2} were mutually different. Copper dendrites formed at an overpotential of 550 mV were very rare, and the copper deposit obtained at this overpotential represented the mixture of cauliflower-like forms and individual dendrites (Fig. 3.18a). On the other hand, the powdered deposit obtained at 700 mV was constructed from very branchy dendrites (Fig. 3.18b). This clear difference in the surface morphology of deposits is confirmed by the very different specific surfaces of these copper deposits.

Hence, it was shown that dendritic deposits showed the largest electrode surface area, i.e., these deposits are of the largest $S_{sp,m}$. This is consistent with Chassaing et al. [80] who showed by impedance spectroscopy that the electrodeposition of ramified deposits was accompanied by the large increase of the deposit surface area.

3.4.2 The Representative Powder Particle and the Particle Size Distribution Curves

As already mentioned, a copper powder is not formed of particles of identical size and morphology; the individual particles may assume

various forms and have very different surface areas for the same average size of granule [3]. For that reason, to relate the powder properties with the deposition process parameters and the deposition conditions, a representative particle of metal powder must be defined, and then, metal powder is defined as a group of identical (i.e. representative) powder particles.

The representative powder particle must have at least one common property with powder as a whole. The specific surface is one such common property characterizing both a metal powder and an individual (representative) powder particle. The specific surface of an individual powder particle can be determined only if its form is approximated by some regular geometric form, such as a cube [60]. On the other hand, numerous methods are available in the literature for the determination of the specific surface of powder, S_{sp} [81].

The representative powder particle is characterized by the same specific surface as a powder consisting of a mixture of different particles. The specific surface of a powder particle, $S_{sp,p}$, is given by

$$S_{sp,p} = \frac{S_{par}}{m_p},\tag{3.33}$$

where S_{par} and m_p are the surface and mass of particle, respectively.

The shape of particle size distribution curve can be calculated assuming that the largest fraction of particles corresponds to the representative ones [60, 67], and one such calculated curve is shown in Fig. 3.21. The shape of this curve was in good agreement with those found in the literature [1, 82].

3.4.2.1 Real Systems

In real conditions, the size and shape of powder particles and hence the particle size distribution curve depend on a regime of electrolysis, a composition of solution, deposition time, cathodic material, temperature, hydrodynamic regime, *etc*.

During electrochemical deposition processes of copper at overpotentials belonging to the plateau of the limiting diffusion
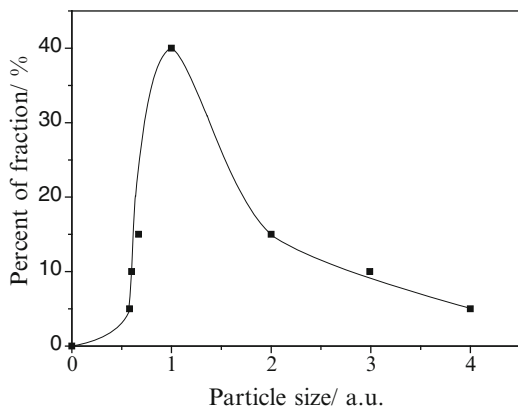
Fig. 3.21 The shape of the typical calculated particle size distribution curve (according to [60, 67])

current density, the shape of powder particles strongly depended on the applied overpotential of electrodeposition. The reason for it is relatively wide range of overpotentials belonging to the plateau of the limiting diffusion current density of about 500 mV. The characteristic of electrodeposition processes in this range of overpotentials is the absence of vigorous hydrogen evolution. The typical particle size distribution curves for copper powders obtained by electrodeposition at overpotentials of 600, 700, and 800 mV on platinum electrodes are shown in Fig. 3.22 [83]. In all results presented here, copper was electrodeposited from 0.10 M $CuSO_4$ in 0.50 M H_2SO_4 at the room temperature. From Fig. 3.22, it can be seen that the increase of overpotential leads to the formation of smaller particles and to narrower particles size distribution curves.

The type of cathodic materials used had strong effect on the shape of particle size distribution curves [6, 83]. For example, at overpotentials of 600 and 700 mV (i.e., at overpotentials belonging to the plateaus of the limiting diffusion current density), smaller particles and narrower distribution curves were obtained for the electrodeposition on a platinum electrode than on an aluminum electrode. This is due to fact that aluminum is covered with a relatively thick oxide film which causes an enlarged ohmic resistance
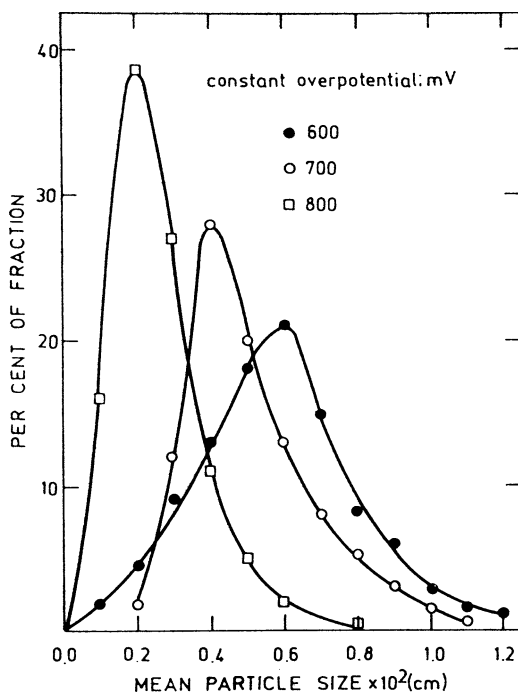
Fig. 3.22 Particle size distribution curves for copper powders obtained by potentiostatic electrodeposition on platinum electrodes (Reprinted from [6, 83] with permission from Springer.)

of the electrode–solution interface of aluminum than the one for platinum [83]. At an overpotential of 800 mV (this overpotential is outside the plateau of the limiting diffusion current density), there was not any difference in particle size distribution curves obtained on platinum and aluminum electrodes. The reason for it is the fact that an overpotential of 800 mV is situated in the hydrogen codeposition range where the process is dominantly controlled by hydrogen evolution reaction.

Anyway, increasing overpotential leads to the formation of a more disperse deposit characterized by the decreased particle size. This can be explained by the fact that increasing overpotential leads to the decrease of the height of protrusion, $h_{0,i}$, at which dendrites start to
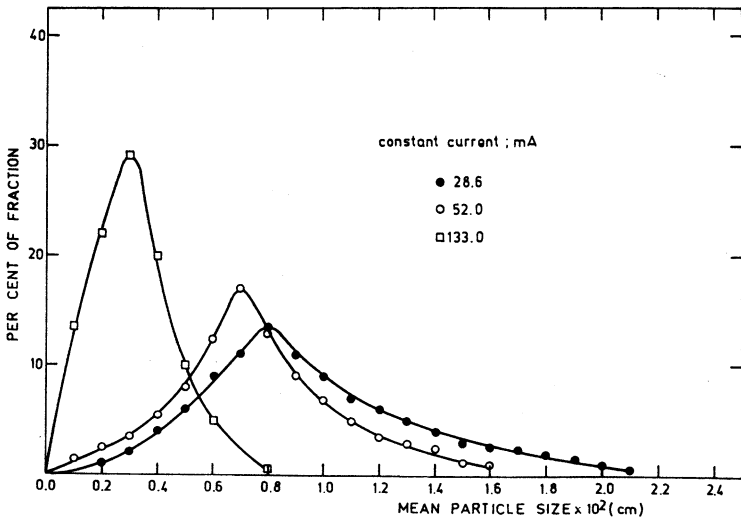
Fig. 3.23 Particle size distribution curves for copper powders obtained by galvanostatic electrodeposition on platinum electrodes. Surface area of the electrode: 0.63 cm^2 (Reprinted from [6, 83] with permission from Springer.)

grow instantaneously. Hence, increasing overpotential means a larger number of growth sites suitable for the growth of dendrites. On the other hand [19], the velocity of dendrite growth is maximum for some optimal value of the dendrite tip radius. The optimal tip radius decreases with increasing overpotential. With the dendrite tip radii larger than the optimal value, the difference between maximal and actual velocities of dendrite growth increases with the increasing overpotential. Hence, smaller particles and narrower particle size distribution curves are expected with the increasing overpotential of powder formation [6, 83].

The particle size distribution curves for copper powders obtained on the platinum electrodes in galvanostatic regime at currents of 28.6, 52.0, and 133 mA are shown in Fig. 3.23. The selected currents corresponded to average currents recorded in potentiostatic electrodepositions at overpotentials of 600, 700, and 800 mV, respectively [83]. The formation of larger particles and less narrow distribution curves in the galvanostatic regime than those formed in the potentiostatic
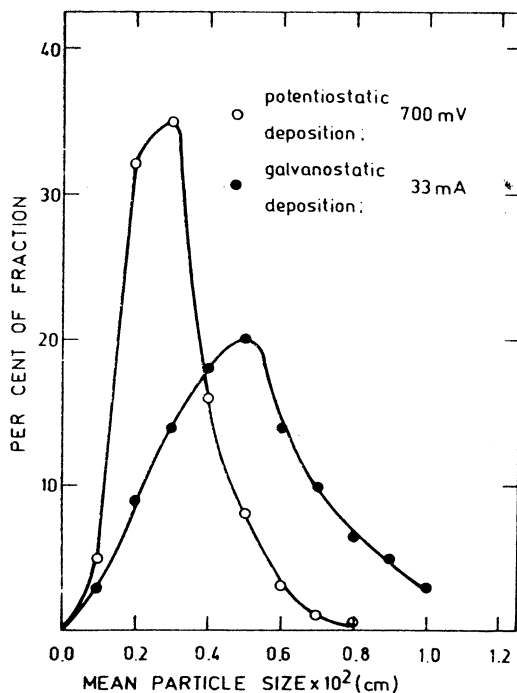
Fig. 3.24 Particle size distribution curves for copper powders obtained by the potentiostatic and galvanostatic (the average current in the potentiostatic regime) electrodepositions on copper electrodes. Surface area of the electrode: 0.63 cm^2 (Reprinted from [83] with permission from Springer.)

regime (Fig. 3.22) can be considered as follows: during electrodeposition in the galvanostatic regime in the hydrogen codeposition range, overpotential is determined by hydrogen reduction, and for the difference of overpotentials of the order 100 mV, ten times larger current of electrodeposition is required. Hence, in real conditions, smaller differences in size of the particles are expected during electrodeposition by different current densities, as well as less narrow particle size distribution curves relative to the ones obtained in potentiostatic electrodeposition. A similar situation was observed when copper was used as a cathode material (Fig. 3.24).

Anyway, the effect of the increasing current density in the galvanostatic electrodeposition is qualitatively same as the increase of overpotential in potentiostatic electrodeposition, and the essence of the particle size distribution curve formation is the same in both the cases.

3.4.3   Correlation Between the Apparent Density and the Specific Surface

The apparent density or volumetric mass is defined as the mass per unit volume of powder [1].

It is well known that copper powders characterized with high values of specific surface exhibit low apparent density. Powder particles from the same fraction of different powders occupy approximately the same volume, while the structure of metallic copper can be considerably different causing different apparent densities and specific surfaces of powder (Fig. 3.15) [61, 62]. Obviously, the more disperse the powder particles are, the smaller the apparent density of the copper powder is and the larger the specific surface is. Factors affecting the apparent density of copper powders are electrolyte composition (copper and acid content), electrolyte temperature, electrolyte circulation rate, current density, and brush-down interval [61].

Using the data of Calusaru [3], the dependence of the apparent density on the specific surface of a copper powder can be determined [60, 67]. The correlation between the apparent density ρ' and the specific surface of a copper powder can be given by (3.34):

$$\rho' = \frac{K}{S_{sp}}, \qquad (3.34)$$

where K is a constant. This constant is determined from the slope of the dependence of $\rho' - 1/S_{sp}$ as $K \approx 1,000 \text{ cm}^{-1}$ [67]. The maximal difference between values of the apparent density determined experimentally and the one calculated using Eq. (3.34) is 20% and less than 10% in other cases. Hence, the apparent density is well correlated

with the specific surface of a copper powder by the use of Eq. (3.34). On the other hand, Eq. (3.34) can be rewritten in the form

$$\rho' S_{sp} = K, \tag{3.35}$$

which means that the value of K can be estimated using the values of specific surface and apparent density of each particular powder.

The relation between the apparent density and the specific surface of powder is very important from the practical point of view. The experimental determination of S_{sp} requires a relatively complicated equipment and experimental procedure, while ρ' can be easily determined. S_{sp} and ρ' depend on many variables: concentration of depositing ion, concentration of the supporting electrolyte, temperature, and stirring rate, and for example, using data from [84], S_{sp} can be satisfactory estimated by the use of Eq. (3.34).

3.4.3.1 The Effect of the Regime of Reversing Current on the Apparent Density of Copper Powder

The strong effect on the apparent density of copper powder can be achieved by the application of periodically changing regimes of electrolysis, such as the reversing current (RC) regime. Generally, the apparent density of powder increases by the selection of appropriate parameters of the RC regimes [62]. Figures 3.25–3.27 show comparative inspection of morphologies of powder particles obtained in the constant galvanostatic regime (DC regime; Fig. 3.25) and by the different RC regimes (Figs. 3.26 and 3.27). It is necessary to note that the current density amplitude in the RC regimes corresponded to the selected current density in the DC regime ($j = 3,600$ A/m^2). The other parameters of electrolysis were same (15 g dm^{-3} CuSO$_4$·5H$_2$O in 140 g dm^{-3} H$_2$SO$_4$; temperature: $(50 \pm 2.0)°$C; electrolyte circulation rate: 0.11 dm^3 min^{-1}) [61]. The decrease of dendritic character and the increase of compactness of powder particles were observed by the application of RC regimes. The effect of this regime is less pronounced in the minute range (Fig. 3.26) than in the second one when agglomerates of monocrystal subparticles were formed (Fig. 3.27). The powder particles obtained by the RC regime in the
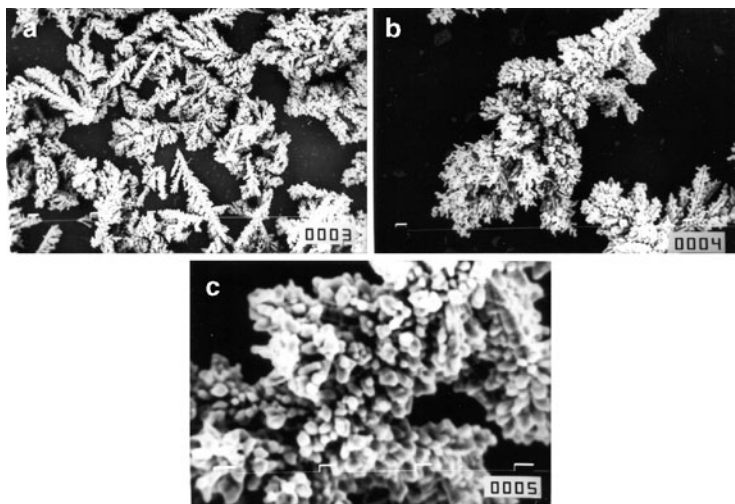
Fig. 3.25 The powder particles obtained by the galvanostatic electrodeposition. The current density: 3,600 A/m^2. Fraction (149–177) μm and apparent density: 0.524 g cm^{-3}. (**a**) ×200; (**b**) ×1000, and (**c**) ×3500. The powder was not sieved (Reprinted from [62] with permission from Serbian Chemical Society.)
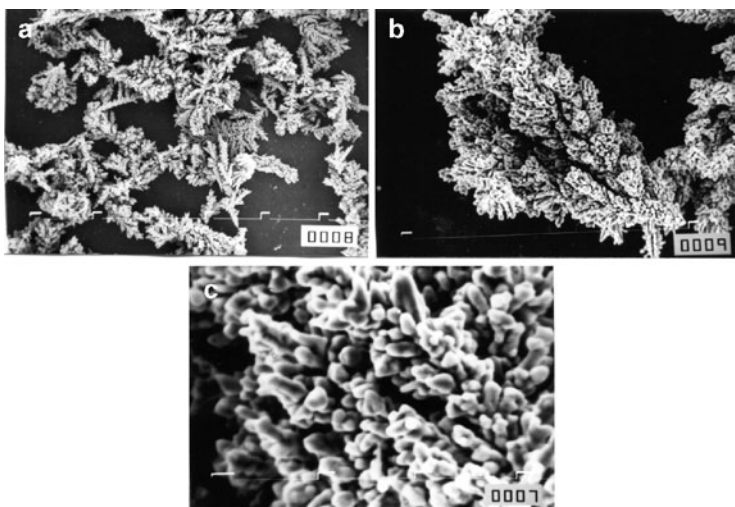

Fig. 3.26 The powder particles obtained by the RC regime. Amplitude current density: 3,600 A/m^2. Cathodic to anodic time ratio: 5. Cathodic pulse duration: 5 min. Apparent density: 0.644 g/cm^3. (**a**) ×200; (**b**) ×1000, and (**c**) ×3500. The powder was not sieved (Reprinted from [62] with permission from Serbian Chemical Society.)
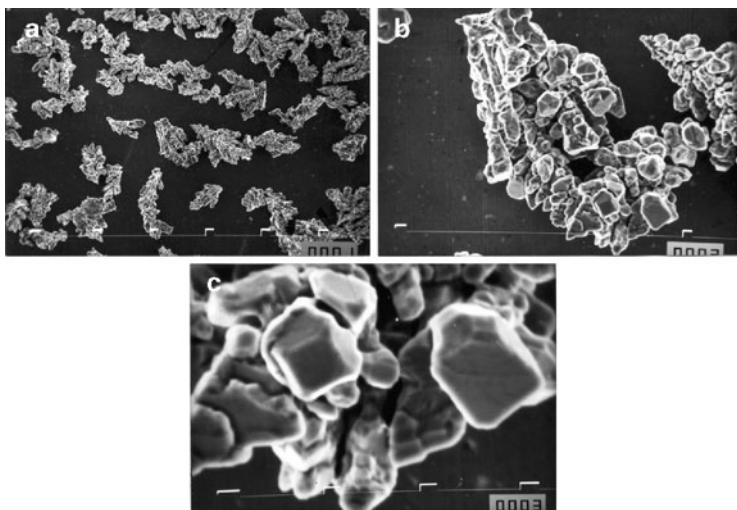
Fig. 3.27 The powder particles obtained by the RC regime. Amplitude current density: 3,600 A/m^2. Cathodic to anodic time ratio: 2.5. Cathodic pulse duration: 1 s. Apparent density: 1.624 g cm^{-3}. (**a**) ×200; (**b**) ×1000, and (**c**) ×3500. The powder was not sieved (Reprinted from [62] with permission from Serbian Chemical Society.)

second range were of considerably larger apparent density (1.624 g/cm^3) than those formed in the minute range (0.644 g/cm^3) and in the constant galvanostatic regime (0.524 g/cm^3).

The increase of the apparent density of powder particles by the application of RC regimes can be explained by the effect of the anodic time in square-waves RC on selective dissolution of the electrode surface [62]. The selective dissolution of the electrode surface during the anodic time only occurs at points with a very small radii of curvature, which dissolve faster than flat parts of the surface or of points with larger tip radii. In the minute range, the duration of selective dissolution must be shorter compared to the overall anodic dissolution time, because the tip radii of dendrites or dendrite branches very quickly become sufficiently large to make the effect of selective dissolution negligible and the particles dissolve uniformly. A decrease of the overall dissolution time leads to a decrease of the

time in which the particles dissolve uniformly and the effect of selective dissolution is more pronounced from the point of view of the Kelvin effect, i.e., the selective dissolution on the particle "macrolevel," making the particles less branched.

On the other hand, the adatoms which are not included completely in the metal lattice will be dissolved faster than those which are included in it, which has the effect of selective dissolution on the "microlevel" of the particle which results in the formation of regular crystal forms. The effect of the decreased dissolution time from the minute to the second range is the same as in the case of the particle "macrolevel." More about the effect of periodically changing regimes of electrolysis on morphology of powder particles was given in the chapter considering morphology of lead and silver powder particles.

3.4.4 The Effect of the Shape and Structure of the Particle on the Flowability of Electrolytic Copper Powder

The flowability of a copper powder depends on the interparticle friction, which is determined by the surface area and surface roughness of the particles. As the surface area and surface roughness increase, the amount of friction in the powder mass increases and the powder exhibits less efficient flow. The same appears with the shape of particle.

The more irregular the shape of particles is, the less efficient the flow of powder is. Resistance to flow is the main feature of friction and it decreases as the particles approach to a smooth spherical shape. The effect of particle size distribution on the powder flowability is also important. If the powder consists of monosized particles which are more or less in mutual point contact, making the contact surface as low as possible, even dendritic deposits can flow. If the powder consists of different particles, the interstitial voids of the larger particles can be filled by the smaller ones, the contact surface area increases, and the flow of the powder is less efficient [1]. As a result

of this, a nonsieved powder often does not flow, while the fractions of the same powder flow [61, 62]. Hence, the best conditions for the free flow of the powder are fulfilled if the powder consists of mono-sized particles of spherical shape with a surface structure approaching to the structure of a smooth metal surface.

For the analysis of the flowability of the powder, due to the existence of nonsieved powders which can flow, the shape and the structure of the powder particles are more important than particle size distribution. Flowability of nonsieved powders occurs when the surface parts of the particles corresponding to the metal segments are larger than or equal to the pores between them [65].

Typical particles of the fraction 149–177 μm of *powders A* and *B* are shown in Fig. 3.15. (*Powder A* was obtained at 1,800 A m^{-2}, while *Powder B* was obtained at 3,600 A/m^2.) The fraction of *powder A* exhibits excellent flowability, while the fraction of *powder B* does not flow. Although the surface structure is very different, in the first approximation, the shape of both particles can be taken as spherical.

Hence, the powder particles can be approximated to be mono-sized and spherical ones. The flow time of fraction 149–177 μm of *powder A* was about 20 s, which corresponds to excellent flowability [61] but the nonsieved powder does not flow due to the fact that the surface structure can allow the jamming of the particles of different fractions. On the other hand, the structure of the particle of fraction 149–177 μm of *powder B* from Fig. 3.15 is very porous and such particles can interweave. Obviously, such behavior leads to the nonflowing powder.

As already shown, the flowability of copper powder is mainly determined by the structure of the surface of the powder particles. The effect of the particle shape is also important, but probably it is not the decisive factor. If the surface structure of powders approaches the structure of the surface of bulk copper and if the shape of the particles approaches a sphere, the friction in the powder mass is low and the flow of the powder is efficient. Besides, in these cases, the particle size distribution will not have an effect on the flowability of the copper powder, so nonsieved powders exhibit free flow.

3.5   Conclusions

There is an important difference between disperse deposits formed in galvanostatic and potentiostatic conditions. In potentiostatic electrodeposition, the properties of disperse deposits mainly depend on overpotential of electrodeposition. The electrodeposition overpotential remains constant during deposition time, as well as the real current density, and the structure of disperse deposits does not change with the electrodeposition time. Hence, it can be expected that both the structure of powder particles and the properties of powder (as association of different powder particles) on the macrolevel do not depend on the electrodeposition time.

In the formation of disperse metals by galvanostatic electrodeposition [75], the apparent current density is constant, while the surface area of a deposit increases during electrodeposition leading to the decrease of both the real current density and the overpotential of electrodeposition. Then, the change of the structure of disperse deposits is observed. In this way, in galvanostatic conditions, the structure of particles can be different in different parts of the one and the same powder particle [85]. Naturally, due to the change of the structure of particles, the properties of powder obtained in galvanostatic electrodeposition will depend on the electrodeposition time. The dependence of the properties of metal powders on the structure of powder particles, and the dependence of metal coatings on the structure of the surface [77, 78, 86–88] are examples of the effects of micro- and submicrostructures on the behavior of the macrosystems.

Electrodeposition at a periodically changing rate offers a number of possibilities for changing the deposition conditions at one and the same deposition rate [43]. In this way, powder particles with different grain size and morphology can be obtained by varying the wave of periodically changing current or overpotential [6]. Electrodeposition at a periodically changing rate is based on the periodic repetition of current or overpotential waves [27, 43]. The most important regime from the theoretical point of view is the regime of pulsating overpotential (PO). On the other hand, the most important regime from a practical point of view is the regime of reversing current (RC).

Copper powders with different apparent densities and related properties were obtained by the change of conditions of electrolysis such as: electrolyte composition (acid and copper content), electrolyte temperature, electrolyte circulation rate, current density, and brush-down interval. Similar effects are expected by changing the parameters which determine the shape of the deposition reversing current wave [6]. Besides, it seems that the surface structure of powder particles obtained in reversing current (RC) electrodeposition is more compact than in the constant galvanostatic regime permitting the free flow of powders with considerably lower apparent densities [62]. This will be considered in more detail in the future.

The relations between the decisive characteristics of metal powder and the conditions of electrodeposition have not been established so far in a semiquantitative way. Hence, electrodeposition of metal powders can be regarded as largely empirical, an activity in which there is much art and little science. We hope that this will change with the publication of this chapter.

The specific surface of copper powder is related to the overpotential of electrodeposition. Also, it is shown that the apparent density is a function of the specific surface of powder, while the flowability of powder is a function of the apparent density. In this way, the most important properties of the powder are related to both the specific surface and the conditions of electrodeposition. Additionally the shape of particle size distribution curve is also discussed qualitatively.

The importance of hydrogen codeposition in copper powder formation is also analyzed in this chapter. Regardless of the fact that all above relations are done, more or less, in a semiquantitative way, this chapter can be considered as the initiation of the qualitative analysis of decisive characteristics of metal powders and their relation with conditions of electrodeposition.

References

1. German RM (1994) Powder metallurgy science, 2nd edn. Metal Powder Industries Federation, Princeton, NJ
2. Pavlović MG, Popov KI (2005) Electrochemistry encyclopedia. http://electrochem.cwru.edu/ed/encycl/
3. Calusaru A (1979) Electrodeposition of metal powders, Materials science monographs. Elsevier, New York
4. Orhan G, Hapci G (2010) Powder Technol 201:57
5. Popov KI, Djokić SS, Grgur BN (2002) Fundamental aspects of electrometallurgy. Kluwer Academic/Plenum, New York
6. Popov KI, Pavlović MG (1993) Electrodeposition of metal powders with controlled grain size and morphology. In: White RE, Bockris JO'M, Conway BE (eds) Modern aspects of electrochemistry, vol 24. Plenum, New York, pp 299–391
7. Hirakoso K (1935) Denkikogaku Kyokoishi 3:7
8. Hirakoso K (1935) Chem Abst 29:5749u
9. Ibl N (1962) Advances in electrochemistry and electrochemical engineering, vol 2. Interscience, New York
10. Ibl N (1954) Helv Chim Acta 37:1149
11. Kudra O, Lerner ME (1951) Ukrain Khim Zh 17:890
12. Kudra O, Gitman E (1952) Elektroliticheskoe Poluchenie Metallicheskiekh Poroshkov, Izd. Akad. Nauk Ukr. SSR, Kiev
13. Ibl N, Schadegg K (1967) J Electrochem Soc 114:54
14. Calusaru A (1957) Revista de Chemie Bucuresti 8:369
15. Atanasiu I, Calusaru A (1957) Studii Cercet Met Bucuresti 2:237
16. Russev D (1981) J Appl Electrochem 11:177
17. Theis G, Fassler C, Robertson PM, Dossenbach O, Ibl N (1981) 32nd ISEMeeting, Dubrovnik/Cavtat, vol 1, p 383
18. Popov KI, Maksimović MD, Trnjančev JD, Pavlović MG (1981) J Appl Electrochem 11:239
19. Barton JL, Bockris JO'M (1962) Proc Roy Soc A268:485
20. Maksimović MD, Popov KI, Pavlović MG (1979) Bull Soc Chim 44:687
21. Maksimović MD, Popov KI, Jović LjJ, Pavlović MG (1979) Bull Soc Chim 44:47
22. Krichmar SI (1965) Electrokhim 1:609
23. Diggle JW, Despić AR, Bockris JO'M (1969) J Electrochem Soc 116:1503
24. Despić AR, Diggle JW, Bockris JO'M (1968) J Electrochem Soc 115:507
25. Popov KI, Despić AR (1971) Bull Soc Chim 36:173
26. Despić AR (1970) Croat Chim Acta 42:265
27. Despić AR, Popov KI (1972) Transport controlled deposition and dissolution of metals. In: Conway BE, Bockris JO'M (eds) Modern aspects of electrochemistry, vol 7. Plenum, New York, pp 199–313
28. Popov KI, Pavlović MG, Maksimović MD (1982) J Appl Electrochem 12:525

29. Popov KI, Krstajić NV, Čekerevac MI (1996) The mechanism of formation of coarse and disperse electrodeposits. In: White RE, Conway BE, Bockris JO'M (eds) Modern aspects of electrochemistry, vol 30. Plenum, New York, pp 261–312
30. Nikolić ND, Popov KI, Pavlović LjJ, Pavlović MG (2006) J Electroanal Chem 588:88
31. Nikolić ND, Popov KI, Pavlović LjJ, Pavlović MG (2007) Sensors 7:1
32. Nikolić ND, Pavlović LjJ, Pavlović MG, Popov KI (2008) Powder Technol 185:195
33. Lowenheim FA (1978) Electroplating. McGraw-Hill Book, New York, St. Louis
34. Wolery TJ (1992) EQ3NR – a computer program for geochemical aqueous speciation-solubility calculations: theoretical manual and user's guide, version 7.0. Lawrence Livermore National Laboratory, Livermore, CA
35. Roine A (1999) HSC chemistry: chemical reaction and equilibrium software with extensive thermochemical database. 4.0. Outokumpu Research Oy, Finland
36. Casas JM, Alvarez F, Cifuentes L (2000) Chem Eng Sci 55:6223
37. Pitzer KS (1991) Activity coefficients in electrolyte solutions, 2nd edn. CRC, Boca Raton, FL
38. Nikolić ND, Popov KI (2010) Hydrogen co-deposition effects on the structure of electrodeposited copper. In: Djokić SS (ed) Electrodeposition: theory and practice. Modern aspects of electrochemistry, vol 48. Springer, Berlin, pp 1–70
39. Nikolić ND, Pavlović LjJ, Krstić SB, Pavlović MG, Popov KI (2008) Chem Eng Sci 63:2824
40. Nikolić ND, Pavlović LjJ, Branković G, Pavlović MG, Popov KI (2008) J Serb Chem Soc 73:753
41. Nikolić ND, Branković G, Pavlović MG, Popov KI (2008) J Electroanal Chem 621:13
42. Nikolić ND, Pavlović LjJ, Pavlović MG, Popov KI (2007) Electrochim Acta 52:8096
43. Popov KI, Maksimović MD (1989) Theory of the effect of electrodeposition at periodically changing rate on the morphology of metal deposition. In: Conway BE, Bockris JO'M, White RE (eds) Modern aspects of electrochemistry, vol 19. Plenum, New York, pp 193–250
44. Li Y, Jia W-Z, Song Y-Y, Xia XH (2007) Chem Mater 19:5758
45. Shin H-C, Liu M (2004) Chem Mater 16:5460
46. Kim J-H, Kim R-H, Kwon H-S (2008) Electrochem Commun 10:1148
47. Nikolić ND, Branković G (2010) Electrochem Commun 12:740
48. Shin H-C, Dong J, Liu M (2003) Adv Mater 15:1610
49. Everhart JL (n.d) Copper and copper alloy powder metallurgy properties and applications. http://www.copper.org/resources/properties/129_6/homepage.html
50. Walker R, Duncan SJ (1984) Surf Technol 23:301

51. Maksimović VM, Pavlović LjJ, Pavlović MG, Tomić MV (2009) J Appl Electrochem 39:2545
52. Owais A (2009) J Appl Electrochem 39:1587
53. Pavlović MG, Pavlović LjJ, Maksimović VM, Nikolić ND, Popov KI (2010) Int J Electrochem Sci 5:1862
54. Djokić SS, Nikolić ND, Živković PM, Popov KI, Djokić NS (2011) ECS Trans 33:7
55. Nikolić ND, Branković G, Pavlović MG (2012) Powder Technol. http://dx.doi.org/10.1016/j.powtec.2012.01.014
56. Nikolić ND, Branković G, Maksimović VM, Pavlović MG, Popov KI (2009) J Electroanal Chem 635:111
57. Nikolić ND, Popov KI, Pavlović LjJ, Pavlović MG (2007) J Solid State Electrochem 11:667
58. Popov KI, Nikolić ND, Rakočević Z (2002) J Serb Chem Soc 67:635
59. Popov KI, Nikolić ND, Rakočević Z (2002) J Serb Chem Soc 67:769
60. Nikolić ND, Krstić SB, Pavlović LjJ, Pavlović MG, Popov KI (2008) The mutual relation of decisive characteristics of electrolytic copper powder and effect of deposition conditions on them. In: Hayashi K (ed) Electroanalytical chemistry research trends. Nova, New York, pp 185–209
61. Pavlović MG, Pavlović LjJ, Ivanović ER, Radmilović V, Popov KI (2001) J Serb Chem Soc 66:923
62. Popov KI, Pavlović LjJ, Ivanović ER, Radmilović V, Pavlović MG (2002) J Serb Chem Soc 67:61
63. Popov KI, Nikolić ND, Rakočević Z (2002) J Serb Chem Soc 67:861
64. Popov KI, Krstić SB, Pavlović MG (2003) J Serb Chem Soc 68:511
65. Popov KI, Krstić SB, Obradović MČ, Pavlović MG, Pavlović LjJ, Ivanović ER (2003) J Serb Chem Soc 68:771
66. Popov KI, Pavlović MG, Pavlović LjJ, Ivanović ER, Krstić SB, Obradović MČ (2003) J Serb Chem Soc 68:779
67. Popov KI, Živković PM, Krstić SB (2003) J Serb Chem Soc 68:903
68. Popov KI, Krstić SB, Obradović MČ, Pavlović MG, Pavlović LjJ, Ivanović ER (2004) J Serb Chem Soc 69:43
69. Popov KI, Krstić SB, Pavlović MG, Pavlović LjJ, Maksimović VM (2004) J Serb Chem Soc 69:817
70. Popov KI, Nikolić ND, Krstić SB, Pavlović MG (2006) J Serb Chem Soc 71:397
71. Nikolić ND, Popov KI, Pavlović LjJ, Pavlović MG (2007) Mater Prot 48:3 (in Serbian)
72. Pavlović MG, Nikolić ND, Popov KI (2003) J Serb Chem Soc 68:649
73. Pavlović MG, Pavlović LjJ, Doroslovački ID, Nikolić ND (2004) Hydrometallurgy 73:155
74. Popov KI, Pavlović LjJ, Pavlović MG, Čekerevac MI (1988) Surf Coat Technol 35:39
75. Popov KI, Pavlović MG, Pavlović LjJ, Čekerevac MI, Remović GŽ (1988) Surf Coat Technol 34:355

76. Popov KI, Maksimović MD, Pavlović MG, Lukić DT (1980) J Appl Electrochem 10:299
77. Nikolić ND, Rakočević Z, Popov KI (2005) Nanostructural analysis of bright metal surfaces in relation to their reflectivities. In: Conway BE, Vayenas CG, White RE, Gamboa-Adelco ME (eds) Modern aspects of electrochemistry, vol 38. Kluwer Academic/Plenum, New York, pp 425–474
78. Nikolić ND, Rakočević Z, Popov KI (2001) J Electroanal Chem 514:56
79. Nikolić ND, Popov KI, Pavlović LjJ, Pavlović MG (2006) Surf Coat Technol 201:560
80. Chassaing E, Rosso M, Sapoval B, Chazalviel J-N (1993) Electrochim Acta 38:1941
81. Schatt W, Wierters KP (1997) Powder metallurgy – processing and materials. European Powder Metallurgy Association, Technical University Dresden, Dresden, p 8
82. Peissker E (1984) Int J Powder Metallurgy Powder Technol 20:87
83. Popov KI, Pavlović MG, Maksimović MD, Krstajić SS (1978) J Appl Electrochem 8:503
84. Pavlović LjJ, Nikolić ND, Popov KI (2000) Mater Sci Forum 352:65
85. Murashova I, Pomosov B (1989) In: Polukarov YuM (ed) Itogi nauki i tehniki, Seria Elektrokhimiya, vol 30. Acad. Sci., Moscow, p 90
86. Nikolić ND, Novaković G, Rakočević Z, Djurović DR, Popov KI (2002) Surf Coat Technol 161:188
87. Nikolić ND, Rakočević Z, Popov KI (2004) J Solid State Electrochem 8:526
88. Nikolić ND, Rakočević Z, Djurović DR, Popov KI (2006) Russ J Electrochem 42:112